THE JOURNAL OF PHYSICAL CHEMISTRY C

Feature Article

pubs.acs.org/JPCC

Utility and Importance of Poisson−Nernst−Planck Immittance-Spectroscopy Fitting Models

J. Ross Macdonald*

Department of Physics and Astronomy, University of North Carolina, Chapel Hill, North Carolina 27599-3255, United States

ABSTRACT: This feature article highlights work done by the author and others since 1953 on the Poisson−Nernst−Planck (PNP) continuum model for analyzing and fitting wide-range immittance-spectroscopy (IS) frequency-response data for unsupported materials with diffusing mobile charge species present. The small-signal PNP approach, one relevant for analyzing data involving ordinary or anomalous diffusion, is particularly important because it leads to estimates of the values of far more physically significant parameters than do other available IS fitting models. Unfortunately, its virtues were not well appreciated until recently, and it has thus not been used as widely as it should be. The present work aims at remedying this lack by providing a thorough description of the strengths and weaknesses of the model, its response possibilities, and its broad applicability. It deals with a neutral species that can fully or partially dissociate into positive and negative charged species of equal concentrations but arbitrary mobilities. The full model, including bulk, mobility, generation-recombination, electrode reaction, and adsorption parameters, is first described, and some of its simplified response functions are presented. It is also incorporated in the free LEVMW complex-nonlinear-least-squares fitting program, making all of its features available for analyzing experimental IS data sets. After a detailed review of relevant theoretical and experimental published work involving the PNP approach, exact graphical responses are presented of progressively more complicated PNP models mostly involving charge of only one sign mobile for all four IS immittance levels. Then it is shown to what degree the various PNP-model responses can be fitted within usual experimental error limits by other more common, but less physically germane continuum, discrete, and empirical models. The positive results of such fitting greatly expand the range of usefulness and applicability of the PNP models. Fits of exact and noisy IS Randles-circuit data sets involving a finite-length Warburg part are compared with those involving different PNP models, and the finite-length-Warburg complex−plane response is discussed and compared with that of the interface part of the PNP response. Finally, some other PNP full and interface response possibilities are discussed and illustrated, and results are presented that involve specific adsorption and adsorption-reaction electrode processes of physical interest to such fields as biology, corrosion, and energy storage. Since a composite PNP fitting model with charges of both signs mobile is shown to exactly fit both exact data sets derived from the ordinary Randles circuit and ones generalized to include additional low- or high-frequency relaxation behavior, its scope and utility for fitting and interpreting experimental data should make it the preferred alternative to most fitting circuits that involve both ordinary resistive and capacitive parameters as well as distributed elements such as finite-length Warburg ones.

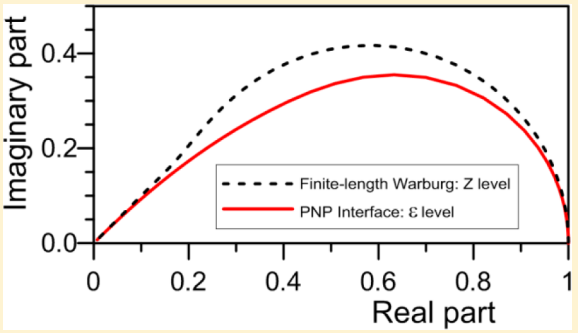

I. INTRODUCTION

This work reviews in detail previous analyses and the current status of important physically realistic models for the fitting and analysis of the frequency response of electrical data of liquid and solid materials involving unsupported diffusing mobile charges, the usual situation for solids. Although all fitting models are necessarily approximate and Feynman rightly said "Experiment is the sole judge of scientific truth", one should also consider Bohr's statement, "Science is not a means of obtaining absolute truth. The real test of a scientific theory is not whether it is 'true' but whether it works".

Here we are interested in models that work, in the sense that they well describe and interpret small-signal impedance-spectroscopy (IS) frequency-response data for a variety of conducting materials. But as D. D. Macdonald[1] cogently pointed out in 2006, one can divide such models into two classes: analog ones, usually instantiated as electrical equivalent circuits that are often only required to fit the data well, and physical ones that additionally account for the physicochemical processes present in the material, particularly those occurring at the interfaces between the electrodes and the material considered. Impedance spectroscopy, or more generally *immittance* spectroscopy, the field where all the fitting models discussed herein apply, is a valuable and extensively used technique for analysis and diagnosis in the areas of electrochemistry, corrosion, batteries, polymers, glasses, biological materials, and many others.[2,3] Therefore it is important to consider physically related models such as the present diffusion-related Poisson−Nernst−Planck (PNP) model, one whose

Received: April 9, 2013
Revised: September 19, 2013
Published: September 23, 2013

virtues are not yet fully appreciated and thus not yet widely used for IS data analysis.

All useful physically appropriate models must satisfy the Kronig−Kramers relations, but even then ambiguity is often present for the first class since more than one different circuit may be found to fit the data equally well. Even the PNP model considered herein involves some ambiguity in the interpretation of some of its physically relevant estimated parameters; see ref 4. Many of the PNP publications cited herein are by J. R. Macdonald or by him and coauthors, and all of these are available for downloading from the Web site http://jrossmacdonald.com. Because the present work includes a considerable number of acronyms and many parameter definitions, lists of those used here are included at the end of this work just before the reference list. The parameter equations included there apply for uniunivalent conditions and equal concentrations of positive and negative charges, but the LEVMW PNP fitting computer program used here is not so restricted.

The distinction between the above two classes defined by D. D. Macdonald may become blurred when a model of interest includes not only some of the R, L, and C elements of ordinary circuit theory but also one or more distributed circuit elements (DCEs), such as a transmission line. They may then require an infinite number of such nondistributed elements to fully describe their response only with such elements. However, useful DCEs, often the result of solution of physically relevant differential equations, may involve such functions as power-laws and hyperbolic tangents and so are readily expressed in simple closed form.

Most useful IS models necessarily involve explicitly or implicitly a bulk high-frequency-limiting real resistance, R_∞ (or resistivity, ρ_∞), and a real capacitance, C_∞ (or dielectric constant, ε_∞), as well as one or more DCEs. Since these high-frequency-limiting bulk parameters are physically significant, the physical significance of any other parameters also present, such as those of DCEs, determines the class into which the resulting composite model falls. For simplicity, we shall here often use just the designation PNP to include both these limiting elements: a resistance in series with the PNP interface DCE and a capacitance in parallel with their combination.

The 1953 small-signal PNP model of ref 5 was the first full solution of the Poisson−Nernst−Planck differential equations for positive and negative mobile charges and involved their complete blocking at identical plane-parallel electrodes separated by a distance L. The PNP designation will often be used here, however, as a general term that also includes (a) the anomalous-diffusion (PNPA) model; (b) one that includes electrode reactions with partial or no blocking (CJPNP); and (c) an extended one including such reactions with specific adsorption (ECJPNP). The PNP-model parameter ψ_A is fixed at unity for the ordinary-diffusion PNP model, and for the PNPA one, $0 < \psi_A < 1$. The ψ_A parameter was denoted ψ in refs 6, 7, and 8 and is different from the ψ of the ordinary-diffusion, comprehensive PNP model of ref 9, one that did not involve such a fractional exponent.

Fitting of relevant immittance data with a PNP model is particularly important because it can lead to estimates of more physically relevant electrical parameters than other available small-signal IS models. Such fitting should preferably use full complex nonlinear least-squares (CNLS), as in the LEVMW computer program freely available at http://jrossmacdonald.com; see Macdonald and Potter, ref 10 and Macdonald, ref 11. The full ECJPNPA model and all of its simplifications are instantiated in Circuit-H of LEVMW. It is available at http://jrossmacdonald.com for fitting experimental data or for generating exact responses, and it was used to produce the results described herein.

In the general binary situation, charge carriers of both signs may be mobile with a mobility ratio, $\Pi_m \equiv \mu_n/\mu_p$, of the mobilities of the negative to positive species of charge, and Π_m will not always be effectively infinite or zero, the one-mobile case. The number of Debye lengths in half the electrode separation is $M \equiv L/(2L_D)$. In most experimental situations, $M \gg 1$. Here we shall consider sinusoidal small-signal immittance data in specific form and will deal primarily with the important uniunivalent one-mobile situation where charges of only one sign are mobile and $M \rightarrow M_1$.

A convenient notation for the six electrode reaction and adsorption parameters needed to specify boundary conditions for mobile charges of both signs follows from the expression given in eq B38 of ref 9. Its principal parameters ρ_j (j = 1 or 2 for positive and negative charges, respectively) are complex when specific adsorption is present (the ECJPNP model), but for electrode reactions only (the CJPNP model) they may be real and frequency independent and then $\rho_j = \rho_{j_0}$, the normalized, dimensionless reaction-rate parameters (NOT resistivities). In past work they have been denoted by (ρ_1, ρ_2) or (ρ_{10}, ρ_{20}), with the latter identification appropriate when these quantities are real. Of particular importance is the (0,∞) choice with negative charges reacting immediately at the electrodes, a CJPNP situation, and the (0,0) completely blocking PNP one. The one-mobile, partially blocking situation with only negative mobile charges usually considered herein is denoted (0, ρ_{20}), with $0 < \rho_{20} < \infty$.

Although the PNP model is a mean-field, conductive-system, effective-medium, continuum one that incorporates the diffusion of point charges inside a possibly nondispersive dielectric medium, it nevertheless well fits many situations involving real charges hopping or diffusing between sites separated by random barriers, as demonstrated later. Further, its fits can lead to estimates of a neutral-species concentration, N_0; equal concentrations of mobile positive and negative charges, c_0, arising from the partial or full dissociation of the neutral species; mobilities and diffusion constants of mobile species; dissociation and recombination parameters; and three reaction and adsorption parameters for each of the two species of mobile charge. Of course, for most fits not all of these many parameters will be found to be simultaneously needed and relevant.

II. SOME PNP EQUATIONS AND DIFFUSION-RELATED PUBLICATIONS

Expressions for the full impedance of the CJPNP and ECJPNP models are included in ref 9, and their generalization to anomalous diffusion appears in refs 6 and 7. Because the CJPNP model involves a neutral species that dissociates into possibly mobile positive and negative charges of arbitrary valence numbers, with partial dissociation (Type A) or full dissociation (Type B), and includes CJ electrode reactions of mobile species, its full formula is too long to include here. However, expressions for some simpler uniunivalent situations are worth listing. For conciseness, it is useful to define the normalized quantities: $Z_{TN} \equiv Z_T/R_\infty$, (or $\rho_{TN} \equiv \rho_T/\rho_\infty$ for data in specific form), where Z_T is the total impedance of the model;

dx.doi.org/10.1021/jp403510y | J. Phys. Chem. C 2013, 117, 23433−23450

$S \equiv i\Omega \equiv i\omega\tau_D$; $\tau_D \equiv R_\infty C_\infty$ is the dielectric relaxation time; $U \equiv S^{\psi_A}$; $P \equiv 1 + U \equiv p^2$; $q \equiv M_1 p$; and $Q \equiv q^{-1}\tanh(q)$. Note that for PNP situations, where $\psi_A = 1$, $U = S$, and P, p, q, and Q all will then be written with a subscript 1. Further, when $\omega \to 0$, Q approaches $M_1^{-1}\tanh(M_1)$.

The following expressions are directly appropriate for situations where charges of a single species are mobile and neutral-species dissociation is either very small or full. Because of an ambiguity discussed in ref 4, however, the present fully blocking results also apply for the usually unlikely, two-mobile case with equal mobilities, when a few parameter values are adjusted to account for the mobilities of both charge species, as shown in Table 3 of ref 4. Also, $M_1 \equiv L/(2L_{D1})$, where L_{D1} is the Debye length appropriate when charge of only one sign is mobile. These conditions avoid the presence of additional low-frequency plateaus in the real part of the resistance for unequal mobilities and similar one-mobile ones associated with a limited range of reasonably large charge dissociation; see especially the results of Figure 4 of ref 6. The PNP (full blocking, ordinary diffusion) expression is then (eq 3 of ref 7)

$$Z_{TN} = (S + Q_1)/SP_1 \tag{1}$$

and that for the PNPA (full blocking, anomalous diffusion) is (eq 6 of ref 7)

$$Z_{TN} = (U + Q)/[UP_1 + (S - U)Q] \tag{2}$$

and the CJPNP (electrode reaction involving negative mobile charges) expression is (eq 7 of ref 8)

$$Z_{TN} = [(S + Q_1) + P_1Q_1\rho_2]/[SP_1 + P_1^2Q_1\rho_2] \tag{3}$$

where $\rho_2 \equiv (L/_2D_2)k_2$, the real, dimensionless electrode-reaction-rate parameter for the mobile charge, whose diffusion coefficient is D_2, and k_2 is the actual rate constant. This equation is still applicable when specific adsorption is present, and ρ_2 is then complex, as in eq 9 of Section VI-C-1.

Since we are dealing with ordinary and anomalous diffusion here, it is worthwhile citing some relevant works involving the diffusion of charge carriers which discuss the physics of such motion from different standpoints. See, for example, Grassberger and Procaccia,[12] Niklasson,[13] Feldman et al.,[14] Nigmatullin and Ryabov,[15] and Havlin and Ben-Avraham.[16] None of these works required the satisfaction of Poisson's equation throughout a solid or liquid medium, however, as does the PNP approach, beginning with that of J. R. Macdonald,[5] although the PNP acronym was not used there. Since the 1950s, the coupled system of Nernst–Planck and Poisson equations has been widely studied and represents the standard model of charge transport in electrolytes and semiconductors.[17]

The PNP designation was probably introduced for the first time in a biophysical workshop by Bob Eisenberg in 1993.[18] He led the application of PNP to steady transport in selective biological ion channels, including various molecular corrections,[19] which significantly modify the flux.[20] Unlike the usual situation discussed herein, where a neutral entity dissociates into positive and negative possibly mobile species, the biological ion-channel PNP analyses involve a separate differential equation for each of the several mobile ionic species present.

A valuable summary that provides much of the history of modeling diffuse-charge dynamics in electrochemical systems is that of Bazant, Thornton, and Ajdari.[21] In contrast to the present work focusing on small-signal PNP impedance, this paper was the first to analyze the nonlinear PNP response to a large voltage step. The analysis was later extended to large ac signals by Olesen et al.[22] and to porous electrodes by Biesheuvel and Bazant.[23] The PNP equations were first modified for large transient voltages in concentrated solutions by Kilic et al.,[24] which led to extensions for induced-charge electrokinetic phenomena[25] and electrochemical kinetics[26] based on nonequilibrium thermodynamics.

III. SELECTIVE HISTORY AND CRITIQUE OF PRIOR PNP WORK

This section provides a history of the development and use of the small-signal PNP diffusion model for the analysis of IS data of nonbiological materials, especially emphasizing work where it has been used in analyzing experimental impedance spectroscopy frequency-response data. A detailed discussion of the limitations of the Nernst–Planck equation appears in R. P. Buck.[27] Not all of them apply, however, to the CJPNP model, and Buck concludes, "Despite its limitations, the Nernst–Planck equation is remarkably useful. It applies to transport in solids, liquids and gels...". Although the PNP model is indeed an approximation, it is useful and important for analyzing IS data from a wide variety of materials, but it doubtless becomes less appropriate for nanosituations where $M < 1$ and for high charge concentrations, particularly because of its assumption of point charges rather than charges of finite size. It should nevertheless be applied in some of these situations to evaluate the limits of its applicability there.

The Nernst–Planck and even Poisson equations have been used to describe and analyze electrochemical response for a century or more, and although they originally considered the possible presence of dc applied potentials (e.g., Jaffé[28] and Mafé et al.[29]), they did not ensure that the Poisson equation applied correctly everywhere. Also, the latter analysis did not refer to the earlier PNP numerical analysis of Macdonald and Franceschetti,[30] which included dc bias and proper satisfaction of the Poisson equation. Even the earlier no-bias, small-signal treatment of Chang and Jaffé[31] (CJ) did not require the Poisson equation to apply everywhere between the electrodes. It did, however, include boundary condition expressions for partial blocking of mobile charges at the electrodes, the ones first incorporated in PNP analysis by Friauf[32] in 1954 and widely used thereafter.

It was not until the publication of the 1953 Macdonald small-signal paper[5] that the Poisson equation was properly included in what later were named the PNP equations. An extension of this work, including dc bias, was given by Franceschetti and Macdonald.[33] Many no-bias small-signal extensions and generalizations of ref 5 have been published by these authors, especially Macdonald[34] and Macdonald and Franceschetti.[9] A valuable summary of the applicability of PNP models for supported and unsupported electrochemical cells was later published by Franceschetti, Macdonald, and Buck.[35]

A remarkable precursor of the PNP approach was the 1899 semi-infinite Warburg diffusion impedance,[36] a constant-phase element (CPE) with a fractional-exponent parameter equal to 0.5, resulting in a slope of magnitude 0.5 in a log–log impedance-level plot. It was later generalized to a finite-length situation and involved a tanh response function involving the same fractional exponent. See the discussion in Section V-F. In turn, in 1985 a tanh expression with its exponent not restricted to a value of 0.5 was proposed by Macdonald [37] but not explicitly identified as involving anomalous diffusion. Later, J.

Bisquert and A. Compte[38] independently introduced such an anomalous diffusion generalization, but it is important to emphasize that none of these diffusion expressions required the satisfaction of Poisson's equation everywhere in a material between two electrodes, and so none of them is a proper solution of the full PNP equations for such a situation.

PNP impedance expressions for complete blocking of mobile charges of both signs[5,9,39] and blocking of mobile charge of one sign and no blocking for the other are presented in ref 40 and are appreciably more complicated for the one-mobile situation than just the finite-length Warburg expression, as evident from eq 1 above. The situation is different for two-mobile situations, however, as discussed in Section VI.

Unfortunately, the PNP model was not often used to fit appropriate data in the period from 1953 to 2010, even though it was available from about 1992 onward as a fitting model in the LEVM computer program and in its current windows version, LEVMW, Circuit-H of the LEVMW Manual. However, in 1982 Franceschetti and Macdonald[41] presented instructive complex−plane PNP impedance plots that included adsorption and reaction electrode effects for electrochromic thin films, and Klein et al.[42] in 2006 published a simplified, $M \gg 1$, approximate version of the one-mobile, fully dissociated PNP model (of actual dielectric-level Debye form: see Section V-A) to allow estimation of mobile-ion concentrations and their mobilities for three different polymers over a range of temperature. These fitting results are discussed in ref 6, where also several one-mobile full PNP models were used to fit IS data for a hydrogel with LEVMW and theoretical PNPA and significant generation-recombination (GR) effects were demonstrated therein.

Several interesting possibilities that can lead to possibly well-separated individual low-frequency plateaus in plots of the real part of the resistivity vs frequency are Faradaic electrode reactions or specific adsorption at electrodes for one or both species of mobile charge, some GR values that effectively mobilize the immobile species of charge, and the presence of actual different mobilities of the two species. Results for the two last possibilities are illustrated in Figure 4 of ref 6.

Also in ref 6 complex−plane, exact normalized dielectric-level plots were compared with "ordinary" diffusion (finite-length Warburg diffusion but erroneously identified in the caption of Figure 1 there as infinite-length Warburg diffusion), with Debye response, with the interface part of PNP response, and with full PNP response. The Warburg and PNP interface responses are similar but differ appreciably at low frequencies, and the full PNP conductive-system response is almost indistinguishable from the Debye relaxation response, matters discussed in more detail in Sections V-A and V-F.

In ref 7, two different generalizations of the PNP model to PNPA ones were compared, and the one discussed in ref 6 and instantiated in the LEVMW PNPA fitting model used in that work was shown to be superior by comparing composite-model fits of IS data for a hydrogel, for the polymer LiTFSI, and for single-crystal $CaCu_3Ti_4O_{12}$(CCTO), an electronic conductor. Various different suggested boundary conditions appropriate for incomplete blocking of mobile charges at the electrodes and incorporated in the PNP differential equations, were next compared in ref 8.

The original Chang-Jaffé[31] boundary conditions of 1952, used in the PNP model to generalize to the CJPNP one,[9,34] do not take explicit account of the Stern inner layer of the double layers at the electrodes as does the Butler−Volmer model. Nevertheless, over the full frequency range for $M \gg 1$, a condition nearly always satisfied in the past and current PNP-model fits of actual unbiased, unsupported experimental data, the CJ and Butler−Volmer conditions were found to be equivalent,[43−46] now a well-accepted result. Further, in ref 46 its IS predictions were shown to be very closely comparable, even for $M = 20$ and in the presence of appreciable currents arising from applied dc bias voltages. In addition, in refs 43−45 detailed results are presented for overpotential-dependent electrode kinetics for both unsupported and supported[43] situations.

In 2005 Bazant, Chu, and Bayly[47] independently considered the $M \gg 1$ condition, termed the Gouy−Chapman one, and its inverse, the Helmholtz $M \ll 1$ one, in detail for PNP models, and the subject was further developed in 2009.[48] These analyses suggested that the Helmholtz condition is particularly applicable for strongly supported situations such as those involving high salt concentrations in water. It is interesting that the 1978 detailed theoretical analysis of ref 45 showed that expressions for diffuse-layer and compact (Stern) ones are mixed in the sense that each involves some parameters from the other layer.

Even when a Stern capacitance parameter has been added in series with the CJPNP model, it has not been found to be relevant for the usual unsupported, unbiased experimental data situation considered herein. It is irrelevant because its value could not be estimated from CJPNP fits of such data. It thus seems likely that when a parallel RC Debye response model is included in series with the usual CJPNP model to represent Stern-layer behavior its contribution to low-frequency behavior usually falls at such low frequencies that they are well below those of the available measurement range because of the very large capacitance of the thin Stern layer. References 47 and 48 provide more valuable results and discussions of the Stern and diffuse layers of the double layer in the presence of nonzero dc currents, but they are not important for the unbiased, flat-band situation of the present PNP analyses and data fitting results. A little known but relevant and important precursor of the later work of Bazant and others mentioned above and that of 2001 in ref 49 appears in ref 50 of 2000, one which independently dealt with a Butler−Volmer reaction-rate situation including Stern layers but point-size ions and treated some nonlinear effects and small-signal frequency-response impedance results at a fixed nonzero bias. It therefore has considerable communality with the results of refs 43−49 and with the earlier numerical analyses of refs 30, 8, and 33.

In ref 8 the response of the CJPNP model was compared with a somewhat different model, the GPNP one, that accounts for partial or no blocking by the addition of a real dc conductance G or conductivity, $\sigma_p \equiv \sigma(0)$, in parallel with the PNP model. The GPNP model fits exact CJPNP data perfectly, but it leads to different estimates of the PNP parameters than the CJPNP ones. However, the σ_p value estimated from a GPNP fit may be used with the value of ρ_∞ to accurately estimate the value of the CJPNP dimensionless reaction-rate parameter, denoted in earlier work by the symbol ρ_2 for one-mobile situations involving mobile negative charges and by k_2 in its dimensional form. These matters are further discussed in ref 8, and the results of CJPNPA one-mobile fits of CCTO data at 80 and 140 K (Krohns et al.[51]) were compared there to investigate possible temperature dependence of the reaction rate.

The paper by L. R. Evangelista et al.[52] considered further PNPA extensions, including memory effects associated with the fractional-time diffusion equation of distributed order, leading to suggestive results which, however, have not been used so far for analysis of actual experimental data. Contemporaneously, Barbero[53] discussed one- and two-mobile, fully dissociated PNP situations in detail and presented expressions for the values of the two real-impedance plateaus that may appear in the two-mobile case, as well as expressions for the frequencies associated with these plateaus.

Then in ref 4 the Barbero work was further discussed, and epsilon-level, rho-level, and sigma-level immittance results for $\log_{10}(\Pi_m)$ mobility-ratio values of 0, 5, and 38 were presented. This paper also identified an ambiguity that can appear in the interpretation of the results of all model fitting of IS data, as well as several other ambiguities specific to PNP models because of their ability to estimate more physically significant parameters than others. One of the latter arises because one-mobile situations and equal-mobility $\log_{10}(\Pi_m) = 0$ two-mobile ones with full blocking lead to the same response shapes but with a few parameter values different by small factors, so their fit results cannot be distinguished without external knowledge. Examples of this ambiguity are presented for the $\log_{10}(\Pi_m)$ values of 0 and 38 for the real-epsilon and the real-rho responses of Figures 1a and 3a of ref 4.

In actuality, there are no real physical one-mobile PNP situations because potential wells and barriers that restrict the free motion of the less mobile of the two charge species present are never infinite, and eventually some of these charges become unbound and free to diffuse/hop. However, the fixed $\log_{10}(\Pi_m) = 38$ choice used here is a good proxy for actual one-mobile behavior because the effects of the resulting small but nonzero mobility of the less mobile species appear at such low frequencies and long times that they fall very far outside the practical range of measurement.

J. L. de Paula et al.[54] recently presented a theoretical PNP treatment of adsorption, generation, and recombination of ions. The adsorption part of the analysis was based on a Langmuir approximation and was said to involve a set of equations different from those appearing in ref 9 and other related work [refs 55, 56, 57, 58, 30, and 59] that involved complex electrode rate constants that generalized the original Chang–Jaffé boundary conditions to account for the simultaneous presence of either or both Faradaic reactions and Langmuir-type specific adsorption, the ECJPNPA model. These general small-signal boundary conditions are designated here as ECJ ones, and some of their consequences are presented later in the present work. The authors of the de Paula paper concluded with the hope that their results would be useful because they showed general response results for "a set of fundamental equations characterizing a continuum diffusional model".

Although the de Paula adsorption boundary equations were overtly different from those in ref 9, eq B38, which also included both reaction and specific adsorption effects, they have been shown, as discussed below, to lead to identical adsorption results. Because the ECJ boundary conditions of eq B38 agree with the basic Butler–Volmer ones in the absence of specific adsorption and for adsorption have been shown to encompass Langmuir behavior as well, possible agreement or disagreement between theoretical ECJ analysis and its adsorption predictions and the adsorption analysis and results of the de Paula work seemed worth pursuing. Therefore, the exact numerical results calculated from the latter approach and presented in its graphs were sent by the corresponding author of that work, Professor L. R. Evangelista, to the present author. They were all then fitted to the PNP model using the LEVMW program with proportional weighting, and "exact" agreement to about thirteen decimal places resulted. Thus, all of the de Paula results are fully consistent with those predicted by the earlier theory, but the work does usefully show some response behaviors not previously depicted. Finally, these results were theoretically reconciled in a subsequent publication.[60] It contains an expression for the PNP impedance of a fully dissociated, two-mobile specific adsorption situation with equal mobilities, one entirely consistent with the LEVMW ECJPNP-model result for such a situation.

The generation-recombination part of the de Paula et al.[54] analysis is consonant with that in refs 5 and 9, but it did not refer to the detailed PNP GR results of ref 6. Those GR results in the de Paula work that did not include adsorption: for example, the data for the red lines in Figures 1 and 2 were also fitted exactly using the $\log_{10}(\Pi_m) = 38$ one-mobile PNP model. However, an additional fit of the same data with the mobility ratio free to vary led to a two-mobile estimate of $\Pi_m \cong 742 \pm 12$, with a small value of the relative standard deviation of the fit residuals, S_F, of about 0.002. In addition, the GR parameter values and that of N_0 were quite different from the one-mobile fit ones.

Although this two-mobile fit was not exact, it was sufficiently good that, had it and the one-mobile one been used with experimental data containing some random errors (real-life situations where S_F is usually no smaller than 0.01), it would have been impossible to choose between the two fits without additional knowledge of the material involved. As one might expect, PNP model fitting evidently does not always allow one to well discriminate between effective motion of an otherwise immobile charged species associated with GR or actual mobility of that species. In fact, for the present two-mobile fit situation, both mechanisms contribute to the response since a second plateau still appears when the two-mobile GR parameter values are used even with the one-mobile Π_m condition.

Diffusion-related studies published by others before 2010 did not usually require satisfaction of the Poisson equation, evidently because of unawareness of the earlier PNP work in the field. In addition, these theoretical results were often not compared with experiment and were not full PNP treatments. However, the de Paula[54] paper discussed above and the Santoro et al.,[61] Lenzi et al.,[62] Ciuchi et al.,[63] de Paula et al.,[64] and Duarte et al.[65] ones all dealt with some aspects of anomalous adsorption and do satisfy the Poisson requirement. The first of these three did not include experimental data fitting, introduced an undefined parameter N, and assumed *equal* values of the diffusion coefficients of positive and negative ions, most unlikely in practice except as a proxy for one-mobile behavior, as discussed in ref 4 and earlier herein.

The 2012 Santoro[61] work provided some plots of the real and imaginary parts of the impedance calculated from a fractional anomalous-diffusion equation, and although it does not mention the limitations of this approach, as discussed in ref 7 and above, it provides useful references to anomalous diffusion work not involving satisfaction of the Poisson equation. The parameter N is evidently the present N_0 with the unstated assumption of full dissociation, so it also denotes the equal concentrations of the mobile ions. The same impedance equation was used in the Ciuchi paper to fit some data for nematic liquid-crystalline electrochemical cells. Its fit

results are significantly different, however, from those for the smectic liquid crystal material included in Table 1 of the slightly earlier[4] publication. The 2011 Lenzi paper[62] usefully cites many references to ordinary or anomalous diffusion in many different materials and uses a fractional diffusion type of PNPA model to analyze IS data for deionized water with electrode boundary condition stated to encompass adsorption and reaction. It did, not, however, cite the earlier results of ref 9 that also do so. It involves complete dissociation of the unidentified mobile ions (of equal assumed mobility) present in the water, and it led to estimated values of both N and diffusion coefficients for two different electrode materials.

The work of ref 65 was also devoted to an IS analysis of pure water data using a generalized ordinary-diffusion PNP-type model involving two groups of fully dissociated positive and negative charges of equal mobilities within each group but with different mobilities for the charges of the two groups. This analysis, which involved no electrode-reaction parameters, led to poorer fits than those of Lenzi, and its fits were also inferior to those of an unpublished separate one-mobile CJPNPA σ-level fit of the ref 65 data by the present author, one that also took account of the increase in σ' data values at the highest few frequencies. Nevertheless, when two groups of different mobile ions are present in a material of interest, the approach of ref 65, further generalized to involve the possibility of free and possibly unequal mobilities of all four charges, would be appropriate. Another generalization, suggested in a private communication from Professor G. Barbero, is the possible need to consider frequency-dependent mobilities in such structured materials as gels. All these possibilities could be incorporated in future PNP models, and data fitting with them might substantiate the need for such extensions.

The later de Paula et al.[64] paper presents theoretical results that take into account both adsorption and generation-recombination effects with a kind of CJPNPA model. While it does mention the earlier extended Chang–Jaffé adsorption work of ref 9, it does not cite the relevant GR work of ref 6. This second de Paula paper involves a model that differs somewhat from the usual CJPNPA model instantiated in LEVMW, and it does not refer to the two-mobile and anomalous diffusion data fits and graphs presented in earlier work[4,6−8,52] using that model. It does, however, show graphical theoretical results very similar to the earlier ones, including some for different mobilities of the positive and negative charge, and it seems likely that, as with the first de Paula paper, much or all of its theoretical and experimental results could be well fitted by the standard model. In its fit of data from a nematic liquid crystal it does not, however, use its model to investigate whether the positive and negative charges had different mobilities but made the usual two-mobile assumption with equal mobilities.

All three of the above publications and most earlier theoretical, diffusion-related ones include plots of the real and imaginary parts of the impedance but do not usually show corresponding results for the admittance and dielectric levels. This is unfortunate since real-part impedance plots may involve two, or possibly even three, low-frequency plateaus. However, it is only at the admittance or conductivity level that one may unambiguously identify an approach to dc response if mobile charges are present and react at the electrodes and if the data extend to sufficiently low frequencies. Even dispersive pure dielectric materials inherently involve a low-frequency real-part impedance plateau,[66] e.g., eq 7 therein.

Therefore, although some of the power-law increases that appear for the real part of the impedance of experimental data at frequencies below those of the ordinary bulk plateau may be associated with anomalous diffusion effects, the presence of actual second or third final low-frequency plateau values usually requires the presence of unequal mobilities, or GR effects, and/or adsorption or reaction processes. Thus, the frequent assumptions of equal mobilities and full dissociation when fitting data with the PNPA model should be avoided. Instead, full ECJPNPA fits with free GR parameters and with a possibly free mobility-ratio parameter are generally needed in general to identify and characterize the one or two lower frequency real-impedance plateau processes that may appear in principle and sometimes in practice.

Unfortunately, none of the 2011−2013 papers mentioned above carried out such full fits of experimental data, and so they did not lead to unambiguous identifications of all the processes leading to their experimental results. A virtue of dealing, as herein, with experimental data transformed to specific form rather than with raw data is that it is then simple to show specific results for all four immittance levels that may allow separate identification of bulk and interface (sometimes called electrode) effects. The results discussed in the next sections further clarify these matters.

IV. EXACT PNP RESPONSES AT ALL FOUR IMMITTANCE LEVELS

In ref 4, two separate types of PNP response are defined: Type A is that with small dissociation, so $c_0 \ll N_0$, while these concentrations are equal for type B, the full dissociation case. Although type-A response is common for solids, type B may be found for low-concentration mobile impurity ions in a dielectric material. In this section, we progressively show how exact type-A one-mobile PNP responses at all four immittance levels change as more and more physical processes and parameters are added to the model. Thus, we compare by pairs PNP and PNPA, PNPA and CJPNPA, and CJPNPA and DCDCJPNPA. Here the composite DCDCJPNPA model is that of a dielectric-level Davidson−Cole one, the DCD, in parallel with the CJPNPA. Although the DCD model was derived empirically, it has been shown[15] that its response may be explained on a physical basis as a discontinuous self-similar process. Further justification for its use in the above combination is discussed below.

The Circuit-H general PNP model available in LEVMW and used to calculate the present one-mobile results includes the following possibly free parameters: N_0, L, Π_m, k_{gr}, ξ, R_1, C_1, ρ_{20}, and ψ_A. For the full CJPNPA model, several other possibly free reaction and adsorption parameters are also available. Here, the k_{gr} and ξ parameters are GR related, with $k_{gr} \equiv k_g/k_r$ and $\xi \equiv \tau_{GR}/\tau_D$, where k_g and k_r are the generation and recombination parameters of papers refs 6 and 9. Further, τ_{GR} and τ_D are the recombination reaction time and the Debye relaxation time, respectively, and ρ_{20} is the dimensionless reaction rate for the mobile negative charge species, named ρ_2 in published work not including specific adsorption. Although ξ is best estimated from a data fit, it often is found to be large. Then it is useful to hold it fixed at a very large value, thus eliminating a free parameter in the fitting.

For the present results, all in specific form, the Circuit-H parameters are $R_1 = \rho_\infty$, $C_1 = \varepsilon_V\varepsilon_\infty$, and $\tau_D = R_1C_1$, where ε_V is the permittivity of vacuum, 8.8542×10^{-14} F/cm. Parameters held fixed are T, the absolute temperature, A, and Π_Z, where A

is the area of an electrode and Π_Z, here unity, is the ratio of the valence numbers of the negative to positive charges, both of concentration c_0. From the values of the fixed and estimated parameters of a fit, LEVMW also calculates values of the indirect quantities defined above, as well as ε_∞, M, mobilities and diffusion coefficients, and the Debye length. Note that, for example, in the present one-mobile case with univalent negative charges mobile $\sigma_\infty \equiv (1/\rho_\infty) \equiv (e\mu_n c_0)(1 + \Pi_m^{-1})$. Although the full frequency-response expression for the CJPNPA model instantiated in LEVMW is too long to list here, the one-mobile CJPNP response formula, eq 3 of Section II, appears in eq 7 of ref 8 for small dissociation conditions. In the zero-frequency limit it leads to $\rho'(0)/\rho_\infty = 1 + (\rho_{20})^{-1}$. Expressions for all CJPNP situations are listed and discussed in ref 9.

To obtain type-A DCDCJPNPA composite model parameters of experimental relevance, I combined and modified unpublished fit results for a smectic liquid crystal which showed both dielectric dispersion, represented by the DCD part of the model, and mobile charge associated with small dissociation of a neutral center, somewhat similar to that found from PNPA fits of CCTO material in refs 7, 8, and 4. Some values found for the latter were modified to yield much smaller diffusion coefficients than those for CCTO to represent the motion of mobile ions rather than that of electrons. Fixed values of T = 305.6 K and L = 0.01 cm were used, as well as $\Pi_m = 10^{38}$. Other PNP and CJPNPA rounded parameter values were $N_0 = 4.305 \times 10^{21}$ cm^{-3}, $k_{gr} = 4.305 \times 10^5$ cm^{-3}, $\xi = 10^{35}$ fixed, $R_1 = 5.925 \times 10^7$ ohm-cm, $C_1 = 2.877 \times 10^{-13}$ F/cm, $\rho_{20} = 0.01$, and ψ_A = 1 or 0.9. Relevant rounded calculated values were $c_0 = 4.305 \times 10^{13}$ cm^{-3}, $\varepsilon_\infty = 3.25$, $M_1 = 151$, $k_g = 5.87 \times 10^{-39}$ s^{-1}, $k_r = 1.36 \times 10^{-44}$ cm^3/s, $\tau_D = 1.70 \times 10^{-5}$ s, $\tau_{GR} = 1.70 \times 10^{30}$ s, $\mu_n = 2.45 \times 10^{-3}$ cm^2/(V s), $D_n = 6.44 \times 10^{-5}$ cm^2/s, with $L_D = 2.34 \times 10^{-5}$ cm for the two-mobile case and 3.31×10^{-5} cm for the present one-mobile one. Here the value of the reaction rate, k_2, calculated from ρ_{20}, was 1.29×10^{-4} cm/s. For the DCD model the parameter values were $\Delta\varepsilon_D \equiv \varepsilon_0 - \varepsilon_\infty = 11.09$, $\tau_{DCD} = 4.03 \times 10^{-8}$ S, and $\gamma_{DCD} = 0.963$. The very large value of τ_{GR} used here ensures that Type-A behavior remains relevant even at the lowest applied frequencies.

The low-frequency-limiting PNP plateau value of $\varepsilon_0 = \varepsilon'(0)$ is $\varepsilon_\infty M_1 = 490.2$, and so $\Delta\varepsilon_D = (M_1 - 1)\varepsilon_\infty$. Therefore, $\rho_\infty = (\tau_D/\varepsilon_V\varepsilon_\infty) = (M_1\tau_D/\varepsilon_V\varepsilon_0)$, the value of the low-frequency ρ' plateau. The often-used empirical Barton–Nakajima–Namikawa (BNN) equation, involving a parameter p with a value usually near unity, has been discussed for several different conductive-system fitting models in ref 67. It may be written as $\sigma_0 = p\varepsilon_V\Delta\varepsilon\omega_p$, where $\omega_p \equiv 2\pi\nu_p$ is the angular frequency of the peak of the $|\varepsilon''(\omega)|$ loss curve. Although the PNP model without electrode reactions involves complete blocking and so its σ_0 is zero, to obtain an *effective* estimate of p for the PNP model let us replace σ_0 in the BNN relation by $1/\rho_\infty$, write the result as an equation for ρ_∞, and set it equal to the above PNP expression for ρ_∞. Then solving for p yields $p = (\varepsilon_0/\Delta\varepsilon)/(M_1\tau_D\omega_p)$. Finally, define $\omega_{PNP} \equiv 2\pi\nu_{PNP} \equiv 1/M_1\tau_D$; then it follows that $p = \{M_1/(M_1 - 1)\}(\nu_{PNP}/\nu_p)$. For the present PNP data the first quotient is 1.00662, and the second is (61.8926/62.0995) = 0.99667. Thus the effective BNN value calculated in this way for the PNP model is here about 1.003, indistinguishable from unity in experimental situations.

Figure 1 shows how PNP responses change to PNPA ones at all four immittance levels when the value of ψ_A is reduced from 1 to 0.9. We see that the major changes occur in the low-frequency responses of ρ' and σ' with the appearance of CPE-like, anomalous diffusion behavior. This behavior, per se, is actually unrealistic since it continues unabated with no approach to plateaus in the low-frequency limit. In actuality, however, any of four different processes mentioned in the last section lead to such plateaus, and for real data one or more of them is always present even when their effects occur at frequencies below the range of measurement. For both the PNP and PNPA models, $\sigma_\infty = 1/\rho_\infty$, and ρ_∞ is the value of the low-frequency plateau in the PNP $\rho'(\nu)$ and of the midfrequency one in the PNPA response.

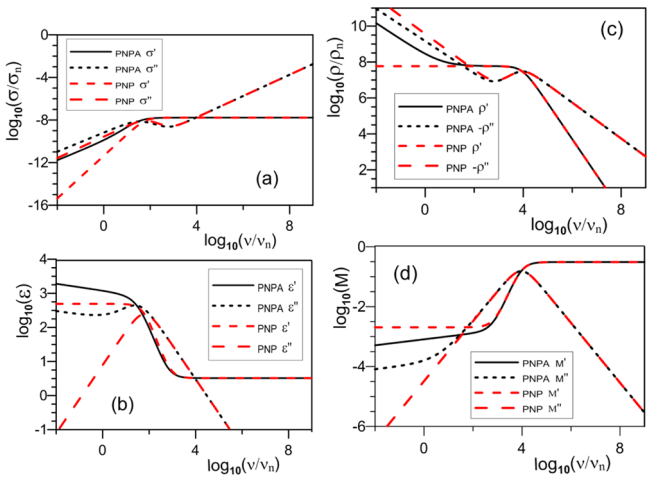

Figure 1. Comparison of log–log PNP and PNPA responses at the (a) σ; (b) ε; (c) ρ; and (d) M immittance levels. Here and elsewhere σ_n = 1 S/cm, ρ_n = 1 Ω cm, and ν_n = 1 Hz. Since ε'' values are negative, they are conventionally shown here and in subsequent figures as positive.

Figure 2 demonstrates the change from PNPA responses to CJPNPA ones. It illustrates the transformation of low-frequency, real-part PNPA complete-blocking behavior to CJPNPA partial blocking involving Chang–Jaffé boundary conditions. Note, however, that no approach to a plateau in ε' is evident. It is particularly important that for the four immittance levels it is only the presence of partial or no blocking of charges at the electrode interface that leads to a final low-frequency-limiting dc plateau in σ'. It is this behavior, not necessarily the presence of a limiting low-frequency plateau in $\rho'(\nu)$, that is characteristic of dc behavior.

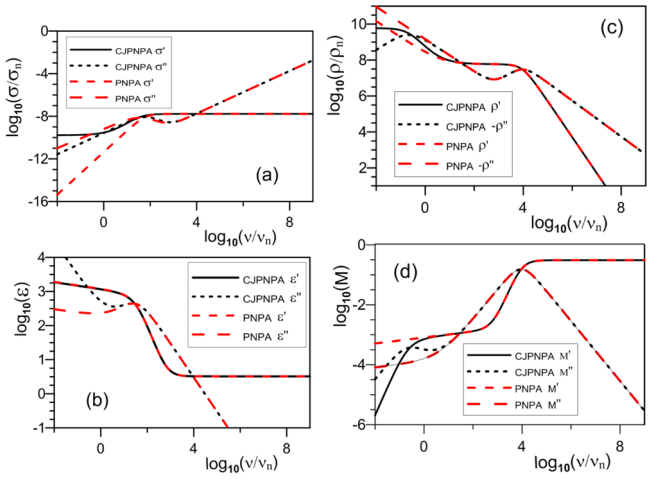

Figure 2. Comparison of log–log PNPA and CJPNPA responses at the (a) σ; (b) ε; (c) ρ; and (d) M immittance levels.

dx.doi.org/10.1021/jp403510y | J. Phys. Chem. C 2013, 117, 23433–23450

The dielectric-level Davidson−Cole model, the DCD, has been found useful for fitting the IS data for a variety of materials; however, as mentioned in Gulich et al.,[68] it is often more appropriate for the higher-frequency parts of the response, and another model needs to be used to represent electrode effects. Here we use the CJPNPA model to account for such interfacial effects. It is interesting, however, that in the absence of anomalous diffusion the ε_0 values for the PNP, CJPNP, and DCDCJPNP models are about 490.2, 480.6, and 491.7, respectively, with the difference between the last two values being just that of $\Delta\varepsilon_D$.

The inclusion of the DCD as part of the full composite model produces further important changes above 10^4 Hz as shown in Figure 3.

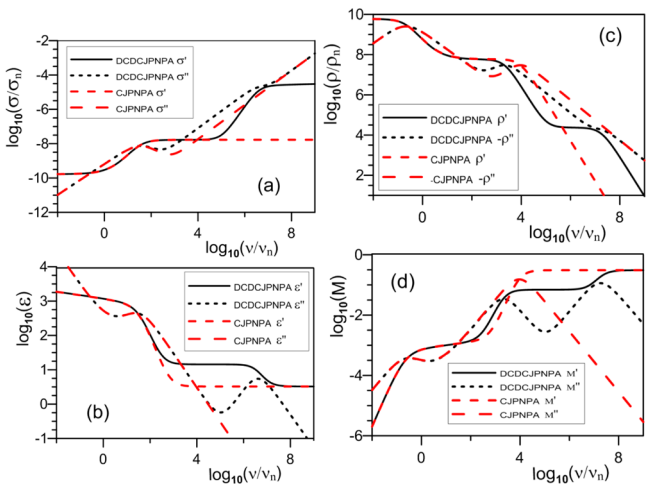

Figure 3. Comparison of log−log CJPNPA and DCDCJPNPA responses at the (a) σ; (b) ε; (c) ρ; and (d) M immittance levels.

Neither the PNPA nor the CJPNPA model leads to any high-frequency increase in σ' above the usual σ_∞ plateau, but most experimental IS results for conductive-system situations show a transition from that plateau to a CPE-like increase,[68,69] sometimes identified as nearly constant loss. At GHz or THz high frequencies, this response in turn may lead to a final high-frequency (boson) peak or plateau associated with pure vibrational effects.[69] Here, for convenience, we have chosen a τ_{DCD} value that causes the intrinsic final DCD plateau to appear at lower frequencies.

V. RESULTS OF FITTING EXACT COMPOSITE PNP-MODEL RESPONSE DATA SETS WITH EMPIRICAL MODELS

A. Fits of PNP Data: Dielectric Models. We start by considering the simple PNP model alone, always involving the one-mobile situation. Although it involves the diffusion of charges and is thus a conductive-system model with fully blocking electrodes, it leads very closely to a semicircular complex−plane plot at the dielectric level, a signature of Debye dielectric behavior, that of the DebD model, a dielectric-system one involving dipoles. This is an example of the Maxwell ambiguity discussed, for example, in ref 4. As shown by Klein et al.,[42] when $M_1 \gg 1$ a DebD expression approximating one-mobile PNP response is

$$\varepsilon/\varepsilon_\infty = 1 + (M_1 - 1)/(1 + iM_1\omega\tau_D) \quad (4)$$

where τ_D is the PNP characteristic relaxation-time parameter. This is a Debye simplification of the usual DCD model

$$\varepsilon(\omega) = \varepsilon_\infty + \Delta\varepsilon_D/(1 + i\omega\tau_{DCD})^{\gamma_{DCD}} \quad (5)$$

when $\gamma_{DCD} = 1$.

With this choice, a DebD fit of eq 5 to the present PNP data yielded the estimates $\varepsilon_\infty = 3.249$, $\Delta\varepsilon_D = 487.2$, and $\tau_{DCD} = 2.561 \times 10^{-3}$ S, with $S_F = 9.5 \times 10^{-4}$ and a value of PDRMS, the RMS average of the relative standard deviations of the free parameter estimates, of 7.1×10^{-5}. For such exceptionally small goodness-of-fit values, it is impossible to distinguish between data and fit values in log−log plots or even in the more sensitive dielectric complex−plane plots. The above fit values agree within three significant figures with those calculated using the PNP M_1 and τ_D values, as in eq 1 of Section II. With γ_{DCD} free to vary, however, the resulting DCD fit led to the results: $\varepsilon_\infty = 3.249$, $\Delta\varepsilon_D = 486.9$, $\tau_{DCD} = 2.564 \times 10^{-3}$ S, and $\gamma_{DCD} = 0.99974$, with $S_F = 4.2 \times 10^{-4}$ and PDRMS $= 3.1 \times 10^{-5}$, a substantially better fit.

Although we cannot readily distinguish between the data and the model fit values, something useful can be learned from the relative residuals of the epsilon-level fits. Define ε_d as that of the data and ε_f as the fit values. Then the relative residual may be defined as $r_\varepsilon \equiv (\varepsilon_d - \varepsilon_f)/\varepsilon_f$. It is one of the LEVMW fit outputs, and its real and imaginary parts are shown in Figure 4.

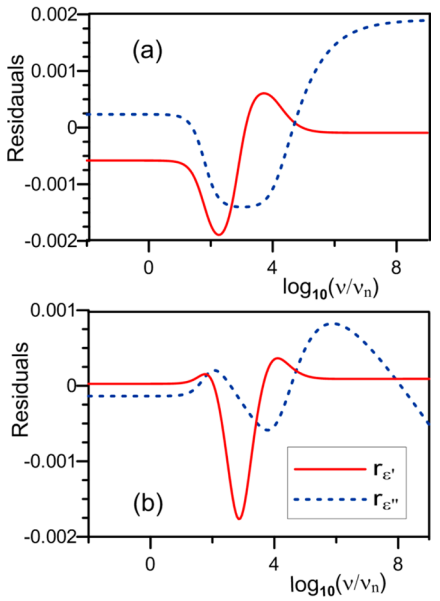

Figure 4. Real-part and imaginary-part relative residuals for (a) the DebD fit of the PNP data (see Figure 1b) and (b) the DCD fit of the data. Note the difference in the two y-axis scales.

These plots show that the very small change from the fixed value of $\gamma_{DCD} = 1$ in (a) to the free value of $\gamma_{DCD} = 0.99974$ in (b) leads to remarkable changes in the relative residuals of the fits. It is evident that the differences inherent in the DebD eq 4 approximation of the PNP model of eq 1 are very small in the low-frequency region below about 10 Hz but that the approximation is somewhat less adequate, especially its real-part fit in the mid-frequency range, even when it is generalized to DCD response, as in eq 5.

B. Fits of PNP Data: Conductive Models. Because the basic PNP model involves complete blocking, fits of its data with another conducting-system model require the inclusion of

dx.doi.org/10.1021/jp403510y | J. Phys. Chem. C 2013, 117, 23433−23450

a series capacitance, C_0. One possibility for such a model is the empirical Havriliak–Negami model (the HNC), which is expressed at the complex resistivity level as

$$\rho(\omega) = \rho_0/[1 + (i\omega\tau_C)^{\alpha_C}]^{\gamma_C} \quad (6)$$

When α_C is set to 1, the HNC model reduces to the conductive-level Davidson–Cole (DCC) one, and when both exponents are fixed at 1, it becomes the conductive-level Debye (DebC) expression. The designation of the HNC with a capacitance C_0 in series with it is HNC·C_0. Note that empirical conducting-system models involve a resistance or resistivity parameter usually associated with a Faradaic electrode reaction of the mobile charge or charges, and they do not allow one to discriminate between one-mobile and two-mobile, equal-mobility, conduction situations. Of course, when a model such as the HNC is used to fit data involving complete blocking (ideal polarization) such as that from the PNP and dielectric situations, its nonzero resistance or resistivity parameter does not represent dc behavior.

A DebC·C_0 fit of the PNP data led to the following estimated values: $\rho_0 = 5.858 \times 10^7$ Ω cm, $\tau_C = 3.271$ s, and $C_0 = 4.340 \times 10^{-11}$ F/cm, with $S_F = 9.5 \times 10^{-4}$ and PDRMS = 7.2×10^{-5}. The first and third parameter values are close to the corresponding PNP ones. This fit leads to an estimate of the BNN p parameter of about 0.988. In contrast, an HNC·C_0 fit yielded the estimates: $\rho_0 = 5.866 \times 10^7$ Ω cm, $\tau_C = 3.271$ s, $C_0 = 4.340 \times 10^{-11}$ F/cm, $\alpha_C = 0.9996$, $\gamma_C = 1.0004$, with $S_F = 2.3 \times 10^{-4}$ and PDRMS = 2.3×10^{-5}. This is still nearly a DebC·C_0 result but a much better fit and a BNN p estimate of 0.989.

C. Fits of PNPA Data: Conductive Models. *1. Empirical Models.* Here a HNC·C_0 model alone is inapplicable because it cannot account for the low-frequency rise above the mid-to-low-frequency ρ' plateau shown in Figure 2(a). The simplest composite model found that fits the PNPA data well may be written C_∞HNC·CPE, where C_∞ represents the high-frequency-limiting dielectric constant ε_∞ and is in parallel with the HNC. The series CPE response function is $\rho_{CPE}(\omega) \equiv 1/[Q_{CPE}(i\omega)^\beta]$. Its exponent satisfies $0 < \beta \leq 1$, and Q_{CPE} is a specific capacitance only when $\beta = 1$.

The composite model fit to the PNPA data led to the estimates: $\rho_0 = 5.864 \times 10^7$ Ω cm, $\tau_C = 0.0337$ s, $\varepsilon_\infty = 3.254$, $\alpha_C = 1.102$, $\gamma_C = 1.0018$, $Q_{CPE} = 1.296 \times 10^{-10}$, $\beta = 0.9001$, with $S_F = 0.0036$ and PDRMS = 4.1×10^{-4}. The ρ_0, ε_∞, and β estimates are comparable to the corresponding PNPA parameter values. The almost exact agreement between the β and ψ_A values confirms that the difference between PNP and PNPA behavior is of CPE power-law character. When γ_C was fixed at unity, thus changing the HNC part of the composite model to the conductive-level Cole–Cole model (CCC), S_F increased slightly to 3.6×10^{-3} with very minor changes to the remaining free parameters. On the other hand, changing to the DCC model led to $S_F = 0.069$ and to $\beta = 0.906$. With both exponents fixed at unity, the DebC model, no good fit was possible, and the PNPA anomalous diffusion behavior was not fitted since the resulting β estimate was the well-determined value 0.9995.

2. Full PNP Model Fit. Finally, it is worth investigating how well the full PNP model, the ECJPNP, is able to fit the present PNPA data in specific form. At least an approximate fit should be possible since, as already mentioned, several different processes can lead to a progressive increase in ρ' as the applied frequency decreases below its midfrequency plateau. The model includes not only arbitrary mobilities but also GR effects and electrode adsorption and reaction ones only for the most mobile charge. We fix ψ_A at 1 and keep the other originally fixed PNPA parameter values the same. The best fit led to the following estimates of those parameter values allowed to be free: $\Pi_m = 2.10 \times 10^3$, $k_{gr} = 4.96 \times 10^6$, $\xi = 1.25 \times 10^4$, $R_1 = 5.941 \times 10^7$ Ω cm, $C_1 = 2.906 \times 10^{-13}$ F/cm, $\rho_{20} = 1.08 \times 10^{-4}$, $\rho_{2\infty} = 1.68 \times 10^{-3}$, and $\xi_{2a} = 8.65 \times 10^4$. Here $\rho_{2\infty}$ and $\xi_{2a} \equiv \tau_{2a}/\tau_D$ are the dimensionless specific-adsorption parameters of eq B38 of ref 9, discussed later for the one-mobile case in eq 9.

The goodness-of-fit parameter values for the above two-mobile PNP fit were $S_F = 0.052$ and PDRMS = 0.064, indicating an adequate but not excellent fit. Although one could not distinguish between the data and fit points for the usual resistivity-level log–log plot, differences were evident, particularly at low frequencies for the more sensitive dielectric-level complex- plane plot. Further, the relative standard deviation of the Π_m mobility ratio was about 0.3, a poorly determined parameter. When this ratio was fixed at the usual one-mobile value of 1[38], $S_F = 0.056$ and PDRMS = 0.028, making it clear that a one-mobile fit was somewhat superior to a two-mobile one. Further, when the reaction rate parameter ρ_{20} was also fixed at zero, the fit-quality values changed to 0.082 and 0.033, respectively, indicating that the presence of a nonzero reaction rate improved the fit somewhat. The estimated value of the concentration of the mobile charge was $c_0 = 1.42 \times 10^{14}$ cm^{-3}, somewhat larger than that of the original PNPA model.

D. Fits of CJPNP and CJPNPA Data Sets: Conductive Models. The DebC·C_0 of the PNP data discussed above in Section V-B needs replacement of the series C_0 parameter by a series resistivity element, ρ_{0S}, and the addition of a parallel capacitance, C_P, representing ε_∞ to make it appropriate for the CJPNP situation. The resulting model may be written as C_PDebC·R_{os}. The fit results using this model are, however, somewhat surprising. They are $\rho_{0S} = 5.936 \times 10^7$ Ω cm, $\rho_{0C} = 5.925 \times 10^9$ Ω cm, $\tau_C = 477.5$ s, and $\varepsilon_\infty = 3.249$, with $S_F = 9.4 \times 10^{-4}$ and PDRMS = 9.7×10^{-5}. We see that the estimated value of the *series* ρ_{0S} is nearly identical to the value of the PNP DebC ρ_0 parameter, and here the DebC resistivity parameter ρ_{0C} is about 100 times larger and takes proper account of the original PNP dimensionless reaction-rate parameter $\rho_{20} = 0.01$. Using the HNC model in place of the DebC one led to results nearly identical to those of the DebC. Although one might have expected the values of the two resistivities to be reversed, the present fit of the CJPNP data requires that the DebC part of the model represents the reaction relaxation process, and no good fit was found with a reversal.

This same behavior was also found when an alternate composite model, consisting of a resistivity in series with a HNC, the C_PHNC·R_{os}, was used to fit the CJPNPA data. The fit of this composite model led to $\rho_{0S} = 5.937 \times 10^7$ Ω cm, $\rho_{0C} = 5.924 \times 10^9$, $\tau_C = 1390$ s, $\alpha_C = 0.9002$, $\gamma_C = 0.9998$, and $\varepsilon_\infty = 3.249$, with $S_F = 9.3 \times 10^{-4}$ and PDRMS = 1.5×10^{-4}. This differs from the above fit of the CJPNP data by the presence of a larger τ_C value and by an α_C value nearly identical to the CJPNPA $\psi_A = 0.9$ value. The addition of a series CPE function to the composite model yields a comparable value of S_F but a very poorly defined estimate of the Q_{CPE} parameter.

E. Fits of the DCDCJPNPA Data. Here it is reasonable to start with a DCDC$_P$HNC·R_{os} fitting model. Its results were $\rho_{0S} = 5.944 \times 10^7$ Ω cm, $\rho_{0C} = 5.925 \times 10^9$ Ω cm, $\tau_C = 1389$ s, $\alpha_C = 0.9000$, $\gamma_C = 0.9999$, $\varepsilon_\infty = 3.249$, $\Delta\varepsilon_D = 11.10$, $\tau_{DCD} = 4.03 \times 10^{-8}$ S, and $\gamma_{DCD} = 0.963$ with $S_F = 1.8 \times 10^{-4}$ and PDRMS = 3.1×10^{-5}. Clearly the DCDC$_P$CCC·R_{os} model is appropriate,

dx.doi.org/10.1021/jp403510y | J. Phys. Chem. C 2013, 117, 23433–23450

and the DCD values are the same as those in the data. The fractional α_C Cole−Cole exponent estimate is exactly that of the PNPA. The DCDCJPNPA LEVMW input file has been added to the LEVMW fitting model as part of its FITTESTS CKT-H file in the Manual. It or any part of it can then be used by anyone to fit appropriate experimental data in specific form. Although its responses are shown in Section IV only for the one-mobile situation, it may also be used with the two-mobile one with equal or different mobilities.

Alternatively, changing the parallel DCD model to a series DCC one yields the all-conductive model, the $C_PHNC{\cdot}R_{os}$·DCC. The DCC part is that of eq 3 with $\alpha_C = 1$ fixed. Fitting led to $\rho_{0S} = 5.940 \times 10^7$ Ω cm, $\rho_{0C} = 5.925 \times 10^9$ Ω cm, $\tau_C = 1389$ s, $\alpha_C = 0.9000$, $\gamma_C = 1.0001$, $\varepsilon_0 = 14.385$, $\rho_0 = 2.33 \times 10^4$ Ω cm, $\tau_{DCC} = 9.19 \times 10^{-9}$ S, and $\gamma_{DCC} = 0.943$, with $S_F = 4.7 \times 10^{-3}$ and PDRMS = 9.0×10^{-4}, a good but much poorer fit than the DCD one. Note also that here the parallel capacitance parameter led to an estimate of the zero-frequency value of the dielectric constant rather than to its high-frequency limit.

F. Fit Summary and One-Mobile Randles Circuit Fits. The fitting results presented above in the present Section V make it clear that the full PNP model with an additional parallel or series element included when necessary can fit virtually all prior experimental IS data previously analyzed with empirical or semiempirical models. These fits, using exact PNP data, are appreciably better than are any fits of experimental data found in the past. Therefore, the choice of which to use for experimental data analyses might be considered unimportant except that the PNP one yields estimates of not only the usual parameters appearing in empirical models but also more physically important ones not involved in such models. The parameters present in the fits discussed above involved only exact PNP data sets restricted to the important one-mobile charge situation because situations where positive and negative charges with unequal mobilities are present are not differentiated in the empirical-model fits. Nevertheless, one may conclude that the full PNP model, including the two-mobile possibility where the above limitation no longer applies, will also be able to well fit much two-mobile experimental data.

Although we have investigated fitting of PNP data by empirical models, one would expect that the conclusions above might well apply to the reverse situation. An important circuit model involving semiempirical parameters is the 1947 Randles one. It originally involved a semi-infinite Warburg element, but soon thereafter that element was replaced by the often more appropriate finite-length Warburg (FLW) one. A general FLW expression is included under "FLW" in the Acronym list. Figure 4.5.7 in the 2005 Impedance Spectroscopy book[2] shows a Randles circuit involving a resistance R_s in series with the parallel combination of a capacitance C_P and a resistance R_{ws} in series with a FLW function involving a resistance R_W and a relaxation time τ_W. Sometimes, τ_W is itself expressed as d^2/D, where d is an effective diffusion thickness and D is a diffusion coefficient parameter, but τ_W is different for one-mobile unsupported situations, one-mobile supported ones, and two-mobile unsupported ones.[35]

Professor Andrzej Lasia kindly sent me in a private communication a data set calculated exactly from the Randles circuit with arbitrarily selected parameter values but with random errors added. These errors were Gaussian distributed of 1-percent size, proportional to the impedance modulus. Here, however, for generality the FLW element is replaced by an extended finite-length one,[37] whose impedance is $Z_W \equiv R_W \tanh[(i\omega\tau_W)^{\psi_W/2}]/(i\omega\tau_W)^{\psi_W/2}$, a model instantiated in LEVMW which reduces to the FLW form when $\psi_W = 1$.

A CNLS fit of the noisy Lasia data set using the Randles circuit model in Circuit-B of the LEVMW fitting program (file RANDLESwithRanErr, available in the LEVMW FITTESTS folder of the Manual for running in LEVMW) led to estimates of the values of the originally unknown six parameters of the full Randles circuit involving this extended Warburg-type element and to $S_F = 0.034$ and PDRMS = 0.011, a reasonably good fit. The rounded values of these R_s, C_P, R_{ws}, R_W, τ_W, and ψ_W estimates suggested that their original values were close to 5 Ω, 20 μF, 50 Ω, 40 Ω, 10 s, and 1, respectively. All these rounded values were indeed the same as those used to generate the data from the circuit. The actual estimate of ψ_W was about 1.001 ± 0.02. The $R'(\nu)$ curve of the Lasia data set is somewhat similar in shape to the CJPNPA one of Figure 3c, but it differs in exhibiting a nonzero high-frequency limiting value of $R_s = 5$ Ω, a midfrequency plateau value of about 55 Ω, and a low-frequency limiting value of about 95 Ω, in agreement with the above estimates.

Next, the unrounded estimates of the fit parameters of the circuit were used to generate an exact data set. Finally, this data set and the original noisy one were each then fitted with the composite R_s·ECJPNPA model with the usual one-mobile choice. It thus included both reaction rate and specific adsorption parameters. Results for the fit of the exact set were $S_F = 0.023$ and PDRMS = 0.046, with a fairly large value of the relative standard deviation of the k_{gr} GR parameter of 0.12. It led to an almost exact estimate of R_s of 5.00 Ω and one of R_{ws} of about 52 Ω, the PNP resistance, and an estimate of ψ_A of 0.966. Its M_1 estimate was about 980; its k_2 electrode reaction rate constant was about 2.4×10^{-4}cm/s; its diffusion constant estimate was 3.1×10^{-5} cm^2/s; and its N_0 and c_0 estimates were 5.57×10^{21} cm^{-3} and 1.03×10^{20} cm^{-3}, respectively, fairly close to complete dissociation. When the two adsorption parameters of the fit were not included, the fit was much worse and led to the results $S_F = 0.078$ and PDRMS = 0.122.

A full R_s·ECJPNPA fit of the noisy data was much poorer: $S_F = 0.28$ and PDRMS = 0.61. Here the k_{gr} parameter could not be estimated, and the estimated uncertainties of the two adsorption parameters were very large. These results show that for the one-mobile PNP model even good Randles circuit data could only be adequately fitted with the inclusion of ECJ specific adsorption parameters, not physically present as part of the data, and that the noisy data set could not be adequately fitted at all. These conclusions are not surprising, however, since one-mobile PNP response is different from finite-length Warburg response for unsupported situations. The situation is even more different, however, when it is assumed that charges of both signs are mobile and at least one of them reacts at the electrodes. See the later discussion and comparison in Sections VI-C-2 and VI-D.

The above difference is particularly obvious when one compares complex−plane FLW and relevant one-mobile PNP responses. The characteristic FLW shape appears in a Z-level plot, but this should be compared here to a dielectric-level PNP one, not, however, to full PNP response which is very close to a Debye semicircle, as shown in Section V-A, but to PNP interface dielectric response. For data and model expressions in specific form the normalized interface conductivity, $\sigma_{iN}(\omega) \equiv \sigma_i(\omega)/\sigma_\infty$, is given for the one-mobile case by eq 40 in ref 9. Its

inverse, ρ_{iN}, may be related to the total PNP complex resistivity, $\rho_{TN}(\omega)$, through

$$\rho_{iN} = [(1 + S)\rho_{TN}(\omega) - 1]/[1 - S\rho_{TN}(\omega)] \quad (7)$$

where as usual $S \equiv i\omega\tau_D$. The result is, for complete or small blocking and full or small dissociation

$$\sigma_{iN} \equiv 1/\rho_{iN} = S(Q_1 - 1)/P_1 \quad (8)$$

where $Q_1 \equiv \tanh[M_1(1 + i\omega\tau_D)^{1/2}]/[M_1(1 + i\omega\tau_D)^{1/2}]$; $P_1 \equiv 1 + S$; and σ_{iN} only reduces to an approximate FLW function at the epsilon level when $|S| \gg 1$and usually $M_1 \gg 1$.

The shape of the dielectric-level PNP high-frequency interface response is the same for the PNP or for the CJPNP model with a small or zero reaction rate, and a normalized shape comparison is provided here in Figure 5. Although the high-frequency limiting slope is the same for both the FLW and the PNP interface function, the midfrequency behaviors are appreciably different, as expected from eq 8. More interface responses are presented in the next section.

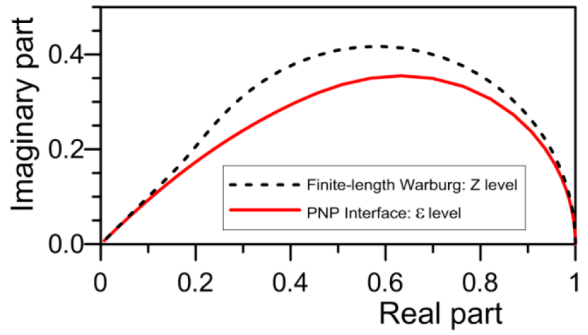

Figure 5. Magnitudes of the complex−plane responses for finite-length Warburg and one-mobile PNP interface functions scaled to real-part maximas of unity.

An unsupported data comparison between a FLW impedance-level formula and a two-mobile PNP one[9] with arbitrary positive and negative charge mobilities was presented in ref 35 and led to their full agreement. The PNP impedance expression used there did not, however, directly include the exact one-mobile limiting situation where the mobility of one charge is zero and that of the other is nonzero or the exact two-mobile situation where charge of one or both signs reacts at the electrodes, and the reaction rate of one of them may be essentially infinite. These possibilities are further discussed in Section VI for full ECJPNP models. They show that Warburg-like impedance-level behavior can appear in two-mobile PNP situations when one charge species is fully blocked and the other is not blocked or only partially blocked, in agreement with earlier results of Figures 1b and 2 of ref 40.

Only part of the full fit parameter results are listed here because full LEVMW input-fit files for the two Randles circuit data fits are now included in the LEVMW FITTESTS CKT-B file of the LEVMW manual, and the two one-mobile R_s·ECJPNPA ones are included in the corresponding CKT-H file. These files may also be used with other experimental data sets to readily make comparisons of the present type and to thus discover which type of model is the more appropriate for the data explored.

VI. VARIOUS PNP-RELATED RESPONSES

A. Interface Responses. Interface response, as calculated from the total response of a PNP model using eq 7, a built-in process in LEVMW, is the part that involves diffusion near the electrodes, and it is thus a crucial element of the full response. Although the epsilon-level PNP complex−plane interface response of eq 8 is presented in Figure 5, more general CJPNP behavior as a function of frequency has not been explicitly included in the earlier plots. Therefore, Figure 6 compares full one-mobile CJPNP behaviors with their interface parts for the four immittance levels.

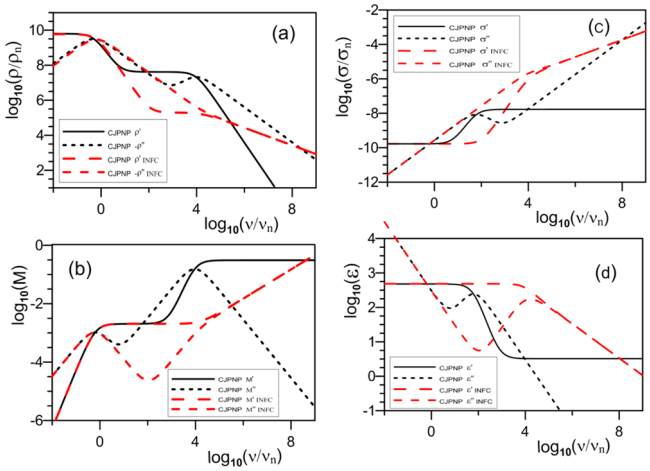

Figure 6. Comparison of full log−log CJPNP responses with their interface (INFC) parts at the (a) ρ, (b) M, (c) σ, and (d) ε immittance levels. Here $M_1 \simeq 150.9$.

As Figure 6 shows, the full and interface responses are almost the same at the lowest frequencies as expected, but the high-frequency limiting interface responses converge to power-law CPE behavior with a fractional exponent of ±0.5, semi-infinite Warburg behavior for large M_1, as is the case here.

B. M_1 Dependences and Other Subjects. The zero-frequency value of $\varepsilon_{TN} \equiv \varepsilon_T/\varepsilon_\infty$ and $\varepsilon_{iN} \equiv \varepsilon_i/\varepsilon_\infty$ for $M_1 \gg 1$ are, as in Figure 6, just M_1 and $M_1 - 1$. However, for any value of M_1, the limiting expressions are M_1ctnh(M_1) and M_1ctnh$(M_1) - 1$. For $M_1 \ll 1$, therefore, they approach the first term of their series expansions, leading to values of 1 and $M_1^2/3$, respectively. Although the shape of the $\varepsilon_{iN}(\nu)$ response remains the same as that shown in Figure 5, the magnitude of the interface response becomes a smaller and smaller part of the full response as the electrode separation L decreases enough to lead to $M_1 \ll 1$. However, one should expect that reducing M_1 at constant L by alternatively increasing the mobile charge concentration will lead, for sufficiently small M_1, to inappropriate results. This will happen because the PNP model's use of point charges does not take proper account of charge-crowding effects at high concentrations.

PNP responses with different M_1 values are readily calculated with LEVMW by varying the electrode separation, L, and probably become progressively less appropriate for $M_1 \ll 1$. Nevertheless, it is worth mentioning results in Figures 5 and 6 of ref 70, an equal-mobility (0,0) situation that involved the original precursor of the LEVM/LEVMW CNLS program. There normalized total impedance and admittance complex−plane plots are presented for several M values in the range $3 \leq M < \infty$. They show that only for M values of the order of 100

dx.doi.org/10.1021/jp403510y | J. Phys. Chem. C 2013, 117, 23433−23450

or more are the low- and high-frequency real-part limiting values good estimates of the normalization quantities. Therefore, in small-M situations R_∞ and its inverse should be estimated by fitting the data with a PNP model rather than from the location where the full-blocking spike appears. Earlier, small and large M results, new finite-length Warburg-like behavior, and discussion of earlier diffusion models published by others that do not require satisfaction of Poisson's equation also appear for (0,0) and (0,∞) equal-mobility situations in the detailed work of ref 55.

Grain-boundary effects are discussed in Chapter 4.1 of the 2005 IS book[2] and for mixed, supported conductors in ref 71, but they will not be discussed here except to suggest that in unsupported cases composite fitting models involving PNP ones might be useful. In a valuable discussion of stimulated dissociation arising from an external source of energy, one that does not, however, ensure that Poisson's equation applies everywhere between the electrodes, Bisquert[72] treats solar-cell situations of practical importance. A full PNP analysis of this situation might well be worthwhile.

C. ECJPNP Reaction and Adsorption/Reaction Responses for One- and Two-Mobile Situations. *1. General Situation.* In Chapter 4.4 of the IS book[2] and in ref 1, D. D. Macdonald shows many complex–plane impedance plots that involve a change of sign of the real and possibly imaginary parts of the impedance as a function of applied dc bias. An important paper by Sadkowki[73] demonstrates that for nonminimum-phase situations of this kind Kronig–Kramers transformation to validate the data may fail when a data set is expressed at the impedance level rather than at the admittance one. Here I consider only small-signal unbiased ECJPNP responses of this type that may be possibly represented by an equivalent circuit with inductive or negative capacitance and negative differential resistance elements, as discussed in detail in ref 58. In Table 2 of that work these elements are related to reaction rate and specific adsorption parameters, ones more physically realistic than are negative resistances and capacitances.

Adsorption/reaction processes can lead to a wide variety of responses, far too many to present here, although some are shown in Figure 3 of ref 43. Thus, we consider here just the three-parameter, Type-B, one-mobile case and the equal-mobility, two-mobile one. In the two-mobile situation, charge of one sign is fully blocked, and the other, here the negative one, may react and possibly adsorb at the electrodes. Then the complex ECJ response expression, eq B38 of ref 9, reduces for the $(0, \rho_{20})$ situation to

$$\rho_2 = [\rho_{20} + i\Omega\xi_{2a}\rho_{2\infty}]/[1 + i\Omega\xi_{2a}] \quad (9)$$

where $\Omega \equiv \omega\tau_D$, and thus $\Omega\xi_{2a} \equiv (\omega\tau_D)(\tau_{2a}/\tau_D) = \omega\tau_{2a}$. Note that an electrode reaction may occur with ξ_{2a} either zero or nonzero even when the adsorption parameter $\rho_{2\infty} = 0$. ξ_{2a} is a normalized relaxation time that can affect the separation between reaction and specific adsorption processes. As usual, the subscript 2 denotes the involvement of a negative charge, and τ_{2a} is its adsorption time constant. Here ρ_{20} and $\rho_{2\infty}$ are dimensionless reaction and specific adsorption rate constants and are not resistivities. An important quantity is $\rho_{nm} \equiv \rho_{2\infty} - \rho_{20}$.

For the one-mobile situation, eqs 1 and 5 involve the FLW-like quantity Q_1 defined below eq 8. However, matters are more complicated for two-mobile situations with equal mobilities. Then two such quantities appear[9,40,55] which we designate here as $Q_{2L} \equiv \tanh[M_2(i\omega\tau_D)^{1/2}]/[M_2(i\omega\tau_D)^{1/2}]$ and $Q_{2H} \equiv \tanh[M_2(1 + i\omega\tau_D)^{1/2}]/[M_2(1 + i\omega\tau_D)^{1/2}]$, ones that become significant at lower and higher frequencies, respectively. A Z_{TN} expression for the (0,∞) situation, one of the choices presented below, appears in eq 2 of ref 40 and is discussed in detail in ref 55 where an equivalent circuit, Figure 18-a (also Figure 1-b in ref 40), is shown to be different from and possibly more appropriate for this situation than is the Randles circuit involving an ordinary FLW element, already discussed in Section V-F. It is also mentioned in ref 55 that the effects of the Q_{2H} term were too small to observe in the high-frequency Warburg-like tail of a dielectric-level normalized complex–plane plot. See the further two-mobile discussion below.

Figure 7 shows results for both one-mobile and two-mobile Type-B ECJPNP $(0, \rho_{20})$ situations, with their details discussed

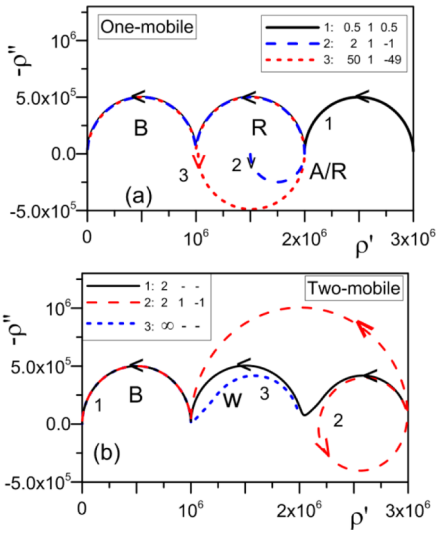

Figure 7. Three complex–plane, specific-impedance ECJPNP responses for (a) one-mobile and (b) two-mobile situations. Arrows show the direction of increasing frequency, and the legends list, for each of the three curves, the values of ρ_{20}, $\rho_{2\infty}$, and ρ_{nm}, respectively.

in the following two subsections. Their frequency range extends from 10^{-3} to 10^8 Hz. Although the plots are presented at the $\rho(\nu)$ level, they involve a value of the specific capacitance of the measuring cell of about 1.4×10^{-10} F/cm, rather than the permittivity of vacuum, to make the transition at $\rho' = 10^6$ Ω cm between the left and the next semicircle approach the imaginary axis closely. The only differences between the results in the (a) and (b) parts of Figure 7 arise from their different choices of the values of the parameters ρ_{20}, $\rho_{2\infty}$, ξ_{2a}, and Π_m. Other parameters were held fixed when the values of any of those listed here were changed, and all their values are provided in the LEVMW input file ECJPNP1M1 included in the Circuit-H FITTESTS file of the LEVMW manual. It was the one used to produce the curve-1 result of Figure 7-a showing three semicircles, and it may be used to generate all of the present results, frequency responses, and other ECJ ones of interest as well.

The value of ρ_∞ for all Figure 7 results was 10^6 Ω cm, and thus the shape of the bulk semicircle at the left does not change when any of the other above-listed parameter values are altered. The ξ_{2a} parameter is only used when $\rho_{2\infty}$ is nonzero. Its value for the one-mobile case was 2×10^6, and it is only used in the two-mobile results for line 2 where its value was 10^6, almost negligibly different when 2×10^6 was used instead.

dx.doi.org/10.1021/jp403510y | J. Phys. Chem. C 2013, 117, 23433–23450

2. One-Mobile Behavior. The three semicircles of line-1 of Figure 7-a show bulk, reaction, and adsorption/reaction behavior where the relevant parameter values have been selected to make the semicircles of nearly equal sizes. For lines 2 and 3, where $\rho_{nm} < 0$, both the real and imaginary parts change signs. Although interesting curves result when the values of either ρ_{20} or $\rho_{2\infty}$ are negative, their physical realizability and significance are dubious.

When the value of ξ_{2a} is much larger than that here, the line-1 R and A/R semicircles merge into a single A/R one spanning the region from 10^6 to 3×10^6 Ω cm, and when ξ_{2a} approaches zero only the B one remains within the available frequency range. In contrast, when $\rho_{2\infty}$ is larger than 1, the R semicircle becomes smaller and the A/R one bigger, but still within the maximum of ρ' not exceeding 3×10^6 Ω cm, and vice versa for smaller values of $\rho_{2\infty}$. Finally, when $\rho_{20} < 0.5$, the A/R semicircle becomes larger, and vice versa for larger values. It disappears when $\rho_{20} = 1$ and ρ_{nm} is zero.

3. Two-Mobile Behavior with Equal Mobilities. It is noteworthy that although no FLW behavior appears for these one-mobile responses it does do so in two-mobile situations. Here line-1 of Figure 7-b also involves three sections, but line-3 exhibits two-section finite-length Warburg-like behavior. When the value of ρ_{20} is greater or less than 2, the middle reaction semicircle becomes smaller or larger than otherwise, as expected, and the size of the third section remains the same. Thus, the reaction semicircle disappears, as in line-3, where the actual value of ρ_{20} was 10^{35}, an excellent approximation to (0,∞) behavior. The sizes of the two responses of line-1 adjoining the bulk one both become smaller when the mobility ratio is greater than 1 and larger when it is smaller. The same behavior results for the remaining finite-length Warburg-like response of line-3.

Line-2 shows the effect of combined A/R processes. When the value of $\rho_{2\infty}$ was reduced to 1.5, the third section no longer shows FLW behavior but instead reduces to an approximate semicircle with a small loop in the region of the transition from the second to third section that extends below zero of the y-axis, as often observed.[1] When the value of ξ_{2a} is larger than that of line-2, the resulting right-most circle becomes smaller, and its center moves to the right. When ξ_{2a} is much smaller, the line-2 behavior approaches and reaches that of line-1 when ξ_{2a} becomes zero. As expected, when the mobility ratio is greater or smaller than 1, the right response is smaller or larger; however, for a value of 0.5, for example, there is an appreciable loop below the y-axis and the positive part of the resulting approximate semicircle extends beyond the present $\rho' = 3 \times 10^6$ Ω cm boundary.

It is noteworthy that the two-section line-3 behavior is of the same general shape as that of Figure 1 of the PNP work of ref 35 and the (0,∞) plot in Figure 2 of ref 40. Except for different normalization, the latter response appears to be essentially the same as that appearing in Figure 2 of ref 74, a 2009 paper involving independent solution of the PNP equations and dealing primarily with electrodiffusion time scales for an equal-mobility, (0,∞), small-signal situation. In that paper the left and right part responses were identified as bulk and Warburg ones, in agreement with their eq 28. Unfortunately, the authors of this work were unfamiliar with the much earlier PNP analyses of refs 5, 55, 40, 34, 9, and 35. In these works, FLW-like behavior was not identified as that of ordinary finite-length-Warburg response and was shown to be more complicated than that in general.

It is easy to fit the exact interface impedance-level (0,∞) CJPNP response of line-3 of Figure 7-b to an actual two-parameter FLW function using the LEVMW CNLS computer program with proportionate weighting. As might be expected from the above discussion, a poor fit was obtained. The impedance-level complex−plane comparison of the exact and fit curves showed close but not exact agreement over a wider high-frequency range than that in Figure 5, but the fitted Warburg part was appreciably smaller at lower frequencies than was the PNP one.

In contrast, it is useful to provide an example where a PNP model involves an interface part that can be well fitted by a FLW function. An input file, CJPNP2MEQ, involving exact data for the equal-mobility, two-mobile situation has now been included in the H-circuit FITTESTS part of the LEVMW program manual, and the fit of its interface part, CJPNPINTFLWFIT, is now also included in the FITTESTS B-Circuit. That two-parameter FLW fit led to values of $S_F = 3.9 \times 10^{-3}$ and PDRMS = 1.9×10^{-4}, good enough that data and fit were indistinguishable in an impedance-level complex−plane graph. However, more helpful results are provided below for the general two-mobile situation with arbitrary mobilities.

D. Extended Randles-Type Circuit Fits: Decoding and Interpretation of Parameters. The Randles impedance-level circuit data set that was analyzed in Section V-F for one-mobile conditions led only to a fair fit and required a nonphysical R_s·ECJPNPA model. It is thus worthwhile to fit the Randles data discussed there with the (0, ρ_{20}) or (0,∞) two-mobile R_s·CJPNP model with arbitrary mobilities. As shown in Figure 2b of ref 9, an appropriate circuit representing the CJPNP model is just a Randles-type one with its FLW element replaced by the CJPNP interface-response model. In this case, the Randles bulk parameters C_P and resistance R_{ws} are identified as C_∞ and R_∞, but fitting of experimental IS data has shown that sometimes the addition of a Debye or Davidson−Cole dielectric model in parallel with a CJPNP or CJPNPA one is needed to adequately fit and interpret the data: for example the DebDCJPNPA or DCDCJPNPA composite models. Therefore, we shall here also fit a Randles exact data set with such composite models as the R_s·DebDCJPNP or R_s·DCDCJPNP models. Note that the DebD part may also be reduced to just a parallel capacitance, C_D.

We start with the six-parameter EXRANONORCLD LEVMW Randles input run file available in the FITTESTS Circuit-O folder of the free LEVMW computer program manual. It spans the frequency region $10^{-6} \leq \nu \leq 10^8$ Hz, involves 20 points per decade, and incorporates the exact Randles circuit data of Section V-F, but the parallel capacitance C_P value used there of 20 μF has been changed to 10 μF. This change was made on the assumption that the Lasia data possibly referred to a half-cell, while here we consider a cell with two identical electrodes at which charge of one sign is completely blocked and that of the other sign, here arbitrarily taken negative, undergoes a fast reaction. Thus, the present value of C_P is the result of two 20 μF capacitors in series. The relevant parameters and their values are thus $R_s = 5$ Ω, $C_P = 10$ μF, $R_{ws} = 50$ Ω, $R_W = 40$ Ω, $\tau_W = 10$ s, and $\psi_W = 1$. With proportional weighting the fit was exact with both S_F and PDRMS about 10^{-13}, the minimum possible value for the LEVMW program. Figure 8, solid line, shows the Randles data in a complex−plane impedance plot.

The first fit of the present exact data set employed the R_s·CJPNP Type-A model with L fixed at 0.1 cm (fit-file

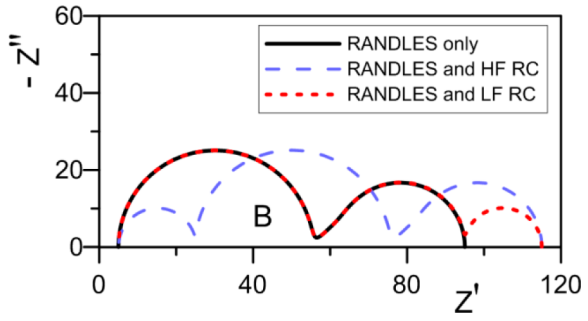

Figure 8. Complex-impedance-plane results for three situations. Solid line: exact Randles circuit data. Long-dash line: Randles response with high-frequency Debye relaxation response in series. Short-dash line: Randles response with low-frequency Debye relaxation response in series.

RanDatRSserCJPNP, available in the FITTESTS H-circuit folder of the LEVMW Manual) and led, with five free parameters, to $S_F = 1.94 \times 10^{-3}$ and PDRMS = 3.06×10^{-4}, with either of the values of N_0 or k_{gr} fixed, but the model was inadequate to allow them both to be free at the same time for this data set. The fit led to estimates of Π_m and R_∞ of 1.26 and 50.3 Ω, respectively. As expected, the C_∞ estimate was very close to 10 μF, but it is unsatisfactory because it leads to an unrealistic estimate of ε_∞ of the order of 10^8!

The second fit therefore used the R_s·DebDCJPNP with its τ_{Deb} relaxation time set so small that the model becomes a R_s·C_DCJPNP one and the C_D capacitance then fits the parallel C_P of the original Randles circuit. Here and in the above fit ρ_2 was fixed at 10^{34}, a good approximation to ∞, and again L was fixed at 0.1 cm. The fit then led to $S_F = 1.8 \times 10^{-11}$ and PDRMS = 4.5×10^{-9} (fit-file EXRANHNORCDeb, also available in the FITTESTS H-circuit file), an essentially exact fit of the seven free parameters except for N_0, k_{gr} and C_∞, whose relative uncertainties were about 8.1×10^{-9}, 8.1×10^{-9}, and 3.4×10^{-9}, respectively, rather than about 10^{-11}. The estimate of C_∞ was about 3.59×10^{-14} F. The estimates of N_0 and c_0 were about 1.95×10^{28} and 6.34×10^{18} cm^{-3}, indeed a type-A situation. When τ_{Deb} was taken as a free parameter, its estimate was 2.06×10^{-11} s with a relative standard deviation of about 0.002, and the fit was about an order of magnitude worse.

In the present situation, the values of A, L, and ε_∞ are all unknown. However, the work of ref 35 leads to the two-mobile Warburg relations $R_\infty/R_W = \Pi_m$ and $\tau_W = L^2/(4D_a)$, where D_a is the ambipolar diffusion constant. It immediately follows from the Randles data values listed earlier that $\Pi_m = 1.25$, the value also obtained from the nearly exact R_s·C_DCJPNP fit discussed above. This important result, not emphasized or explicitly discussed in ref 35, allows the estimation of a Π_m mobility ratio value without the need for fitting to a model whenever unsupported data lead to bulk and Warburg responses such as those in Figure 8, ones widely observed for such conditions.

Using the definitions of D_a and R_∞ in the parameter list below, when values of A and L are known, as is generally the case in IS measurements, one can then calculate values of the concentration c_0 and the diffusion coefficients using just the Randles parameter values. In the present fit with fixed $L = 0.1$ cm, the results are consistent with this value and lead to a value of A of 0.1 cm^2, so A and L are numerically equal. Fitting of the Randles data with a larger value of L leads to the same equality, and with $L = 1.25$ cm, for example, the estimated value of ε_∞ was at least slightly larger than unity. Usually in IS measurements, the numerical value of A/L is appreciably larger than unity, so evidently the choices of parameters made in the original Lasia data do not lead to a very reasonable value of this ratio; however, the data nevertheless are more than adequate to demonstrate how such Randles responses may be analyzed without and with model fitting.

Sometimes a RC DebD circuit is added in series with a Randles one, as in Figure 4.5.8 of ref 2. There it is added to represent the low-frequency effects of a passivating layer on the electrodes, but it can also model the effect of a Stern inner layer. Alternatively, a DebC or DCC circuit may be included to represent the often observed rise in the real part of the admittance at high frequencies, as discussed in refs 68, 69, and 75. These low- and high-frequency response additions are included in Figure 8. The resistance value used in both was 20 Ω, and the high-frequency one involved a relaxation rate parameter value of 10^{-6} s, while it was set at 1000 s for the low-frequency one. The additional low-frequency RC behavior is thus present below 10^{-3} Hz and the high-frequency one above 10^5 Hz. Since most experimental IS data do not extend much below 10^{-3} Hz, passivating effects may indeed be present in this range; however, much lower frequencies would be required to observe Stern-layer capacitive ones, and none has been required in usual IS experimental data set analyses.

VII. SUMMARY AND FUTURE POSSIBILITIES

Many papers using the PNP model to fit relevant experimental data have been reviewed and compared herein, but more such fitting should be carried out. The importance and breadth of application of the general PNP charge-diffusion model have been demonstrated by showing that even with its simplification to charges of a single sign mobile it can fit data generated by a wide range of widely used empirical models previously employed to fit an extensive variety of experimental immittance-spectroscopy data sets. As shown here, however, a composite model including both the PNP and an additional high-frequency response one is needed for analyzing data including CPE-like behavior at high frequencies since the PNP alone includes just bulk response and interface response involving ordinary or anomalous diffusion.

Full and interface responses have been compared for all four immittance levels, as well as some electrode reaction and combined specific adsorption and reaction ones. Fitting results using the ECJPNP model lead to estimates of the values of many more physically significant parameters describing small-signal, unsupported, experimental data than do other models. Further, the two-mobile behavior with arbitrary mobilities includes impedance-level, finite-length, ordinary, or generalized Warburg-like response, especially when charge of at least one sign is not fully blocked at the electrodes.

The complete PNP fitting model is freely available and includes situations where charge species of both signs may be mobile, may involve different valences, and can react and adsorb at the electrodes. Its use can thus show whether charges of both signs or those of only a single sign are mobile, as well as quantifying mobility values. It also allows discrimination between effective charge mobility arising from generation-recombination hopping effects and actual continuum charge mobility. Interestingly, a composite two-mobile PNP model has been shown to lead to an exact fit of data calculated from a Randles circuit involving a FLW dispersive element. Further, its results demonstrate that a complex−plane impedance-level plot of such unsupported experimental data, which shows both a

resistive semicircle and a FLW response as in Figure 8, allows one to accurately estimate the mobility ratio Π_m without the need for any fitting whatsoever.

Future PNP models should involve at least two separate groups of positive and negative charges of arbitrary mobilities and valences to explore and quantify the need for such added complexity and to allow comparison with the alternative of a single PNP model and another conductive-system one in parallel, such as the DCC, to take account of the effects of mobile impurity ions. Finally, it may be appropriate to generalize PNP models to include the possibility for some materials of frequency-dependent mobilities. Much work still remains to be done to continue to show that even an approximate continuum IS model such as the PNP can be more useful than many other hopping and other models at representing experimental IS data and leading to parameter value estimates of physical significance.

AUTHOR INFORMATION

Corresponding Author

*E-mail: macd@email.unc.edu.

Notes

The authors declare no competing financial interest.

Biography

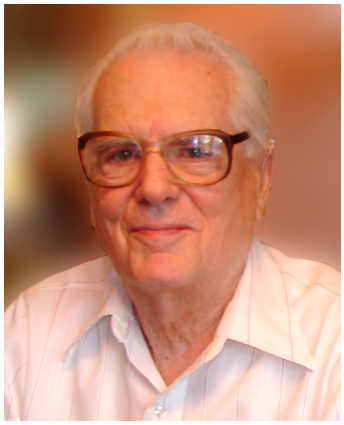

James Ross Macdonald (b. 1923) received the BA degree in Physics from Williams College, the SB and SM degrees in electrical engineering from MIT, and the DPhil and DSc degrees in condensed matter physics from Oxford University, where he was a Rhodes Scholar. Thereafter, he carried out research at Armour Research Foundation, Argonne National Laboratory, and Texas Instruments. At TI he became Director of the Physics Research Laboratory, the Central Research Laboratories, and then became VP for R&E. After taking early retirement from TI in 1974, he was named the William Rand Kenan Jr. Professor of Physics at the Department of Physics and Astronomy of the University of North Carolina, Chapel Hill. He became emeritus in 1989 but has continued to write scientific papers and review them for many journals. He is a member of the National Academies of Engineering and of Science, and he received the Pake Prize of the American Physical Society in 1985 and the IEEE Edison Gold Medal in 1988. He helped pioneer the field of impedance spectroscopy, made freely available the first complex nonlinear least-squares impedance spectroscopy data fitting computer program, and has been a major developer of models for fitting and analyzing such data. More information and all his scientific papers are available at the website http://jrossmacdonald.com.

ACKNOWLEDGMENTS

I owe a large debt to those who have corresponded with me, made creative suggestions, published relevant papers, and provided data for analysis since I began my later PNP work in 2010. A partial list includes G. Barbero, E. Barsoukov, M. Z. Bazant, R. S. Eisenberg, L. R. Evangelista, A. Lasia, and E. K. Lenzi. It is a great pleasure to thank them for their creative and fostering work in nurturing the grapes of knowledge in the PNP immittance spectroscopy vineyard. The resulting wine is available for all.

ACRONYMS AND ABBREVIATIONS

BNN	Barton−Nakajima−Namikawa conductive-system empirical relation
CCC	Cole−Cole dispersive model: conductive level
CCD	Cole−Cole dispersive model: dielectric level
C_DCJPNPA	Composite model: capacitance C_D and CJPNPA in parallel
CELCAP	Capacitance in Farads of the empty measuring cell
CJ	Chang-Jaffé
CJPNP	Poisson−Nernst−Planck model with CJ boundary conditions
CJPNPA	Poisson−Nernst−Planck anomalous-diffusion model with C−J boundary conditions
CNLS	Complex nonlinear least-squares
CPE	Constant-phase DCE element
DCC	Davidson−Cole dispersive model: conductive level
DCD	Davidson−Cole dispersive model: dielectric level, eq 5
DCDCJPNPA	Composite model: DCD and CJPNPA in parallel
DCE	Distributed circuit element
DebC	Debye relaxation model defined at a conductive IS level (one relaxation time)
DebD	Debye relaxation model defined at the dielectric IS level (one relaxation time)
ECJPNP	Extended Poisson−Nernst−Plank diffusion model with electrode reaction and adsorption boundary conditions
FLW	Finite-length-Warburg response function: $Z_W(\omega) \equiv R_W[\{\tanh(i\omega\tau_W)^{0.5}\}/(i\omega\tau_W)^{0.5}]$
GPNP	Composite PNP model including a parallel conductance or conductivity
GR	Generation-recombination; $k_{gr} \equiv k_g/k_r$; see Section IV
HNC	Havriliak−Negami empirical dispersive model: conductive level, eq 6
HND	Havriliak−Negami empirical dispersive model: dielectric level
INFC	Interface part of a PNP model
IS	Immittance or impedance spectroscopy. Immittance denotes all or any of the four levels of raw data (or specific data): impedance, Z; electrical modulus, M; admittance, Y; and complex dielectric constant, ε
LEVMW	Windows version of the original CNLS fitting program LEVM
PDRMS	The root-mean-square value of the relative standard deviations of the estimated values of the free model parameters of a CNLS fit

PNP	Poisson−Nernst−Planck ordinary-diffusion model
PNPA	Poisson−Nernst−Planck anomalous-diffusion model
Type A	PNP response model with small dissociation of a neutral species: $c_0 \ll N_0$
Type B	PNP response model with full dissociation: $c_0 = N_0$

Definition of Principal Parameters

A	Area in cm^2 of each of the identical electrodes
CELCAP	$(A/L)\varepsilon_V$, in Farads
c_0	Concentration of mobile positive and negative charges, in cm^{-3}
C_∞	High-frequency-limiting bulk capacitance of measured material, $(A/L)\varepsilon_\infty\varepsilon_V$
D_i	Diffusion coefficients: positive mobile charges $D_1 = D_p$; negative mobile charges $D_2 = D_n$
D_a	Ambipolar diffusion coefficient: $2D_nD_p/(D_n + D_p)$, in cm^2/s
ε_V	The permittivity of vacuum, 8.8542×10^{-14} F/cm
ε_∞	The high-frequency-limiting dielectric constant of the measuring cell material
L	Separation in cm of the identical electrodes
L_{Dj}	Debye length in cm; $j = 1$, one-mobile; $j = 2$, two mobile: $[\varepsilon_\infty K_B T/(je^2c_0)]^{0.5}$
M_j	$(L/2L_{Dj})$: one- and two-mobile dielectric-ratio quantities
N_0	Concentration in cm^{-3} of a neutral species that partly or fully dissociates into positive and negative species of equal concentration
P,Q,S,U	Normalized dimensionless parameters: defined in Section II
Π_m	$\equiv D_2/D_1 \equiv \mu_2/\mu_1$
Q_{CPE}	Argument of the constant phase element function
R_∞	High-frequency-limiting resistance in ohms of the measuring cell materials; $(L/A)/[ec_0(\mu_n + \mu_p)]$
ρ_2	Normalized, dimensionless reaction rate for negative charges; $\rho_2 \equiv (L/2D_2)k_2$, where k_2 is the reaction rate in cm/s. See eq 9 for specific adsorption complex form
ρ_∞	Specific high-frequency limiting resistivity: $(A/L)R_\infty$ (Ω cm)
S_F	Standard deviation of the relative residuals of a CNLS fit
σ_∞	Specific conductivity: $(1/\rho_\infty) \equiv (e\mu_nc_0)(1 + \Pi_m^{-1})$ in S/cm
T	Absolute temperature (K)
μ_i	Mobilities: positive mobile charges $\mu_1 = \mu_p$; negative mobile charges $\mu_2 = \mu_n$, in $cm^2/(V\ s)$
Z_T	Total impedance of a model; often expressed per unit electrode area
Z_{iN}	Normalized interface impedance: $Z_i/R_\infty \equiv \rho_i/\rho_\infty$
Z_{TN}	Normalized total impedance: $Z_T/R_\infty \equiv \rho_T/\rho_\infty$

REFERENCES

(1) Macdonald, D. D. Reflections on the History of Electrochemical Impedance Spectroscopy. *Electrochim. Acta* **2006**, *51*, 1376−1388.

(2) *Impedance Spectroscopy-Theory, Experiment, and Applications*, 2nd ed.; Barsoukov, E., Macdonald, J. R., Eds.; John Wiley & Sons: NJ, 2005.

(3) Barsoukov, E., Macdonald, J. R. Electrochemical Impedance Spectroscopy. In *Characterization of Materials*, 2nd ed.; Kaufmann, E. N., Ed.; John Wiley & Sons: New York, 2012; pp 1−16.

(4) Macdonald, J. R. Three to Six Ambiguities in Immittance Spectroscopy Data Fitting. *J. Phys.: Condens. Matter* **2012**, *24* (175004), 1−11.

(5) Macdonald, J. R. Theory of AC Space-Charge Polarization Effects in Photoconductors, Semiconductors, and Electrolytes. *Phys. Rev.* **1953**, *92*, 4−17.

(6) Macdonald, J. R. Utility of Continuum Diffusion Models for Analyzing Mobile-ion Immittance Data: Electrode Polarization, Bulk, and Generation-Recombination Effects. *J. Phys.: Condens. Matter* **2010**, *22* (495101), 1−15. Equation A.12 in the Appendix is incorrect but was not used in calculating any numerical results in this work. See pp 4−26 in the LEVMW Manual for the correct equation.

(7) Macdonald, J. R.; Evangelista, L. R.; Lenzi, E. K.; Barbero, G. Comparison of Impedance Spectroscopy Expressions and Responses of Alternate Anomalous Poisson-Nernst-Planck Diffusion Equations for Finite-Length Situations. *J. Phys. Chem. C* **2011**, *115*, 7648−7655.

(8) Macdonald, J. R. Effects of Various Boundary Conditions on the Response of Poisson-Nernst-Planck Impedance Spectroscopy Analysis Models and Comparison with a Continuous-time Random-walk Model. *J. Phys. Chem. A* **2011**, *115*, 13370−13380.

(9) Macdonald, J. R.; Franceschetti, D. R. Theory of Small-signal AC Response of Solids and Liquids with Recombining Mobile Charge. *J. Chem. Phys.* **1978**, *68*, 1614−1637.

(10) Macdonald, J. R.; Potter, L. D, Jr. A Flexible Procedure for Analyzing Impedance Spectroscopy Results: Description and Illustrations. *Solid State Ionics* **1987**, *23*, 61−79.

(11) Macdonald, J. R. Comparison of Parametric and Nonparametric Methods for the Analysis and Inversion of Immittance Data: Critique of Earlier Work. *J. Comput . Phys.* **2000**, *157*, 280−301.

(12) Grassberger, P.; Procaccia, I. The Long time Properties of Diffusion in a Medium with Static Traps. *J. Chem. Phys.* **1982**, *77*, 6281−6284.

(13) Niklasson, G. A. Fractal Aspects of the Dielectric Response of Charge Carriers in Disordered Materials. *J. Appl. Phys.* **1987**, *62*, R1−R14.

(14) Feldman, Y.; Kozlovich, N.; Nir, I.; Garti, N. Dielectric Relaxation in Sodium Bis(2-ethylhexyl)sulfosuccinate-Water-Decane Microemulsions Near the Percolation Temperature Threshold. *Phys. Rev. E* **1995**, *51*, 478−491.

(15) Nigmatullin, R. R.; Ryabov, Y. A. Cole-Davidson Dielectric Relaxation as a Self-similar Relaxation Process. *Phys. Solid State* **1997**, *39*, 87−90.

(16) Havlin, S.; Ben-Avraham, D. Diffusion in Disordered Media. *Adv. Phys.* **2003**, *51*, 187−292.

(17) Markowich, P. A.; Ringhofer, C. A.; Schmeiser, C. *Semiconductor Equations*; Springer-Verlag: New York, 1990.

(18) Eisenberg, R. S. From Structure to Permeation in Open Ionic Channels. *Biophys. J.* **1993**, *64*, A22−A22.

(19) Eisenberg, R. S. Crowded Charges in Ion Channels. In *Advances in Chemical Physics*; John Wiley &Sons, Inc.: New York, 2011; pp 77−273.

(20) Gillespie, D.; Nonner, W.; Eisenberg, R. S. Coupling Poisson−Nernst−Planck and Density Functional Theory to Calculate Ion Flux. *J. Phys.: Condens. Matter* **2002**, *14*, 12129−12145.

(21) Bazant, M. Z.; Thornton, K.; Adjari, A. Diffuse-charge Dynamics in Electrochemical Systems. *Phys. Rev. E* **2004**, *70* (021506), 1−24.

(22) Olesen, L. H.; Bazant, M. Z.; Bruus, H. Strongly Nonlinear Dynamics of Electrolytes in Large AC Voltages. *Phys. Rev. E* **2010**, *82* (011501), 1−29.

(23) Biesheuvel, P. M.; Bazant, M. Z. Nonlinear Dynamics of Capacitive Charging and Desalination by Porous Electrodes. *Phys. Rev. E* **2010**, *81* (031502), 1−12.

(24) Kilic, M. S.; Bazant, M. Z.; Ajdari, A. Steric Effects on the Dynamics of Electrolytes in Large Applied Voltages: II. Modified Nernst-Planck Equations. *Phys. Rev. E* **2007**, *75* (021503), 1−11.

(25) Bazant, M. Z.; Kilic, M. S.; Storey, B. D.; Ajdari, A. Towards an Understanding of Induced-charge Electrokinetics at Large Applied Voltages in Concentrated Solutions. *Adv. Colloid Interface Sci.* **2009**, *152*, 48−88.

(26) Bazant, M. Z. Theory of Chemical Kinetics and Charge Transfer based on Nonequilibrium Thermodynamics. *Acc. Chem. Res.* **2013**, *46*, 1144−1160.
(27) Buck, R. P. Kinetics of Bulk and Interfacial Ionic Motion: Microscopic Bases and Limits for the Nernst-Planck Equation Applied to Membrane Systems. *J. Membr. Sci.* **1984**, 1−62.
(28) Jaffé, G. Theory of Conductivity of Semiconductors. *Phys. Rev.* **1952**, *85*, 354−362.
(29) Mafe, S.; Pellicer, J.; Aguilella, V. M. Ionic Transport and Space Charge Density in Electrolytic Solutions as Described by Nernst-Planck and Poisson Equations. *J. Phys. Chem.* **1986**, *90*, 6045−6050.
(30) Franceschetti, D. R.; Macdonald, J. R. Numerical Analysis of Electrical Response: Statics and Dynamics of Space-Charge Response at Blocking Electrodes. *J. Appl. Phys.* **1979**, *50*, 291−302.
(31) Chang, H.; Jaffé, G. Polarization in Electrolytic Solutions. I. Theory. *J. Chem. Phys.* **1952**, *20*, 1071−1077.
(32) Friauf, R. J. Polarization Effects in the Ionic Conductivity of Silver Bromide. *J. Chem. Phys.* **1954**, *22*, 1329−1338.
(33) Franceschetti, D. R.; Macdonald, J. R. Numerical Analysis of Electrical Response: Biased Small-Signal A.C. Response for Systems with One or Two Blocking Electrodes. *J. Electroanal. Chem.* **1979**, *100*, 583−605.
(34) Macdonald, J. R. Theory of Space-Charge Polarization and Electrode-Discharge Effects. *J. Chem. Phys.* **1974**, *58*, 4982−5001. **1974**, *60*, 343 (correction).
(35) Franceschetti, D. R.; Macdonald, J. R.; Buck, R. P. Interpretation of Finite-Length-Warburg-Type Impedances in Supported and Unsupported Elecrocemical Cells with Kinetically Reversible Electrodes. *J. Electrochem. Soc.* **1991**, *138*, 1368−1371.
(36) Warburg, E. Ueber das Verhalten Sogenannter Unpolarisirbarer Elektroden gegen Wechselstrom. *Ann. Phys. Chem. (Ser. 3)* **1899**, *67*, 493−499.
(37) Macdonald, J. R. Frequency Response of Unified Dielectric and Conductive Systems Involving an Exponential Distribution of Relaxation Times. *Phys. Rev.* **1985**, *58*, 1955−1970.
(38) Bisquert, J.; Compte, A. Theory of the Electrochemical Impedance of Anomalous Diffusion. *J. Electroanal. Chem.* **2001**, *499*, 112−120.
(39) Macdonald, J. R.; Small-Signal, A. C. Response of an Electrochemical Cell with Completely Blocking Electrodes. *J. Electrochem. Soc.* **1988**, *135*, 2274−2279.
(40) Macdonald, J. R. The Impedance of a Galvanic Cell with Two Plane-Parallel Electrodes at a Short Distance. *J. Electroanal. Chem.* **1971**, *32*, 317−328.
(41) Franceschetti, D. R.; Macdonald, J. R.; Small-Signal, A-C Response Theory for Electrochromic Thin Films. *J. Electrochem . Soc.* **1982**, *129*, 1754−1756.
(42) Klein, R. J.; Zhang, S.; Dou, S.; Jones, B. H.; Colby, R. H.; Runt, J. Modeling Electrode Polarization in Dielectric Spectroscopy: Ion Mobility and Mobile Ion Concentration of Single-Ion Polymer Electrolytes. *J. Chem. Phys.* **2006**, *124* (144903), 1−8.
(43) Franceschetti, D. R.; Macdonald, J. R. Electrode Kinetics, Equivalent Circuits, and System Characterization: Small-Signal Conditions. *J. Electroanal. Chem.* **1977**, *82*, 271−301.
(44) Franceschetti, D. R.; Macdonald, J. R. Comment on the Small-Signal AC Response of Solid Electrolytes. *Phys. Status Solidi A* **1977**, *43*, K169−K173.
(45) Franceschetti, D. R.; Macdonald, J. R. Compact Double Layer Effects in Small-Signal Electrical Response. *J. Electroanal. Chem.* **1978**, *87*, 419−422.
(46) Franceschetti, D. R.; Macdonald, J. R. Coupling of Electrode Kinetics and Space Charge Dynamics in Unsupported Systems. *Proc. Third Symposium on Electrode Processes*; Bruckenstein, S., McIntyre, J. D. E., Miller, B., Yeager, E., Ed.; Boston Mass., 7 May 1979, 1980 Proceedings; Vol. *80*−*3*, pp 94−114.
(47) Bazant, M. Z.; Chu, K. T.; Bayly, B. J. Current-Voltage Relations for Electrochemical Thin Films. *SIAM J. Appl. Math.* **2005**, *65*, 1463−1484.
(48) Biesheuvel, P. M.; van Soerstbergen, M.; Bazant, M. Z. Imposed Currents in Galvanic Cells. *Electrochim. Acta* **2009**, *54*, 4857−4871.
(49) Bonnefont, A.; Argoul, F.; Bazant, M. Z. Analysis of Diffuse-Layer Effects on Time-Dependent Interfacial Kinetics. *J. Electroanal. Chem.* **2001**, *500*, 52−61.
(50) Bonnefont, A.; Argoul, F.; Bazant, M. Z. Asymptotic Analysis of Diffuse-Layer Effects on Time-Dependent Interfacial Kinetics. *arXiv.cond-mat/0006104v1*, **2000**, 7 June, 1−22, but available in pdf format at this address in 2008. It overlaps some of the work of ref 49 but contains early impedance results not included there.
(51) Krohns, S.; Lunkenheimer, P.; Ebbinghaus, S. G.; Loidl, A. Broadband Dielectric Spectroscopy on Single-crystalline and Ceramic $CaCu_3Ti_4O_{12}$. *Appl. Phys. Lett.* **2007**, *91* (022910), 1−3.
(52) Evangelista, L. R.; Lenzi, E. K.; Barbero, G.; Macdonald, J. R. Anomalous Diffusion and Memory Effects on the Impedance Spectroscopy for Finite-length Situations. *J. Phys.: Condens. Matter* **2011**, *23* (485005), 1−5.
(53) Barbero, G. One Sign Ion Mobile Approximation. *J. Chem. Phys.* **2011**, *135* (234505), 1−5.
(54) de Paula, J. L.; da Cruz, J. A.; Lenzi, E. K.; Evangelista, L. R. Immittance Response of an Electrolytic Cell in the Presence of Adsorption, Generation, and Recombination of Ions. *J. Electroanal. Chem.* **2012**, *682*, 116−120.
(55) Macdonald, J. R. Electrical Response of Materials Containing Space Charge with Discharge at the Electrodes. *J. Chem. Phys.* **1972**, *54*, 2026−2050. **1972**, *56*, 681 (correction).
(56) Macdonald, J. R. Complex Rate Constant for an Electrochemical System Involving an Adsorbed Intermediate. *J. Electroanal. Chem.* **1976**, *70*, 17−26.
(57) Macdonald, J. R.; Jacobs, P. W. M. Some Aspects of Polarization in Ionic Crystals with Electrode Reactions. *J. Phys. Chem. Solids* **1976**, *37*, 1117−1123.
(58) Franceschetti, D. R.; Macdonald, J. R. Electrode Kinetics, Equivalent Circuits, and System Characterization: Small-Signal Conditions. *J. Electroanal. Chem.* **1977**, *82*, 271−301.
(59) Macdonald, J. R.; Franceschetti, D. R.; Lehnen, A. P. Interfacial Space Charge and Capacitance in Ionic Crystals: Intrinsic Conductors. *J. Chem. Phys.* **1980**, *73*, 5272−5293.
(60) Evangelista, L. R.; Lenzi, E. K.; Barbero, G.; Macdonald, J. R. On the Equivalence Between Specific Adsorption and Kinetic Equation Descriptions of the Admittance Response in Electrolytic Cells. *J. Chem. Phys.* **2013**, *138* (114702), 1−5.
(61) Santoro, P. A.; de Paula, J. L.; Lenzi, E. K.; Evangelista, L. R. Anomalous Diffusion Governed by a Fractional Diffusion Equation and the Electrical Response of an Electrolytic Cell. *J. Chem. Phys.* **2011**, *135* (114704), 1−5.
(62) Lenzi, E. K.; Fernandes, P. R. G.; Petrucci, T.; Mukai, H.; Ribeiro, H. V. Anomalous-Diffusion Approach Applied to the Electrical Response of Water. *Phys. Rev. E* **2011**, *84* (041128), 1−5.
(63) Ciuchi, F.; Mazzulla, A.; Scaramuzza, N.; Lenzi, E. K.; Evangelista, L. R. Fractional Diffusion Equation and the Electrical Impedance: Experimental Evidence in Liquid-Crystalline Cells. *J. Phys. Chem. C* **2012**, *116*, 8773−8777.
(64) de Paula, J. L.; Santoro, P. A.; Zola, R. S.; Lenzi, E. K.; Evangelista, L. R.; Ciuchi, F.; Mazzulla, A.; Scaramuzza, N. Non-Debye Relaxation in the Dielectric Response of Nematic Liquid Crystals: Surface and Memory Effects in the Adsorption-Desorption Process of Ionic Impurities. *Phys. Rev. E* **2012**, *86* (051705), 1−8.
(65) Duarte, A. R.; Batalioto, F.; Barbero, G.; Neto, A. M. F. Electric Impedance of a Sample of Dielectric Liquid Containing Two Groups of Ions Limited by Ohmic Electrodes: A Study with Pure Water. *J. Phys. Chem. B* **2013**, 2985−2991.
(66) Macdonald, J. R. Surprising Conductive- and Dielectric-System Dispersion Differences and Similarities forTwo Kohlrausch-related Relaxation-time-distributions. *J. Phys.: Condens. Matter* **2006**, *18*, 629−644. The word "imaginary" on the third line of p. 643 should be replaced by "real".

(67) Macdonald, J. R. Addendum to 'Fundamental Questions Relating to Ion Conduction in Disordered Solids.'. *J. Appl. Phys.* **2010**, *107*, 101101: 1−9.
(68) Gulich, R.; Köhler, M.; Lunkenheimer, P. Dielectric Spectroscopy on Aqueous Electrolytic Solutions. *Radiat. Environ. Biophys.* **2009**, *48*, 107−114.
(69) Lunkenheimer, P.; Loidl, A. Response of Disordered Matter to Electromagnetic Fields. *Phys. Rev. Lett.* **2003**, *91* (207601), 1−4.
(70) Macdonald, J. R.; Garber, J. A. Analysis of Impedance and Admittance Data for Solids and Liquids. *J. Electrochem . Soc.* **1977**, *124*, 1022−1030.
(71) Jamnik, J. Impedance Spectroscopy of Mixed Conductors with Semi-Blocking Electrodes. *Solid State Ionics* **2003**, *157*, 19−28.
(72) Bisquert, J. Theory of the Impedance of Electron Diffusion and Recombination in a Thin Layer. *J. Phys. Chem. B* **2002**, *106*, 325−333.
(73) Sadkowski, A. CNLS fits and Kamers-Kronig Validation of Resonant EIS data. *J. Electroanal. Chem.* **2004**, *573*, 241−253.
(74) Rubinstein, I.; Zaltzman, B.; Futerman, A.; Gitis, V.; Nikonenko, V. Reexamination of Electrodiffusion Time Scales. *Phys. Rev. E* **2009**, *79* (021506), 1−6.
(75) Macdonald, J. R.; Ahmad, M. M. Slopes, Nearly Constant Loss, Universality, and Hopping Rates for Dispersive Ionic Conduction. *J. Phys.: Condens. Matter* **2007**, *19* (046215), 1−13.